Elsevier Editorial System(tm) for Geomorphology
Manuscript Draft

Manuscript Number:

Title: Evidence of recent ruptures in the central faults of the Acambay graben (Central Mexico)

Article Type: SI: PATA-days spec. volume

Keywords: Temascalcingo fault system; Tepuxtepec fault system; paleoseismology; fault complexity

Corresponding Author: Ms. María Ortuño, doctor

Corresponding Author's Institution: Facultat de Geologia Universitat de Barcelona

First Author: María Ortuño, doctor

Order of Authors: María Ortuño, doctor; Ona Corominas; Pilar Villamor; Ramón F Zúñiga; Pierre Lacan; Gerardo Aguirre-Díaz; Hector Perea; Petra Štěpančíková ; María Teresa Ramírez-Herrera

Abstract: The Acambay Graben, within the central part of the Trans-Mexican Volcanic Belt, is one of the major sources of continental earthquakes in Mexico. Paleo-earthquake activity is well documented for boundary faults, also source of historic earthquakes. However, the activity and paleoseismological history of the axial faults of the graben are not well constrained so far. We provide morphological, structural and sedimentological evidence for the seismogenic nature of two of the axial structures, the Temascalcingo and the Tepuxtepec fault systems. Faults consist of multiple, parallel, 3- to 25-km-long scarps with en echelon and horse-splay patterns. Fault systems extend for 60 km and displace Quaternary to Upper Miocene volcanic materials, fluvial-lacustrine sediments and slope deposits. Observed minimum throws of Upper Miocene and Pliocene markers reach 120-225 m along individual traces. The long-term (0.06 ± 0.02 mm yr-1, minimum) and short-term (0.12 ± 0.02 mm yr-1) slip rate of the Temascalcingo fault system present similar values. Only the long-term slip rate (0.01-0.02 mm yr-1, minimum) of the Tepuxtepec system could be constrained. The Holocene fault rupture history at two sites provided evidence for six ruptures since 12,500-11,195 BC. Three of those ruptures occurred between 11,847 ± 652 BC and 11,425 ± 465 BC. Variable single event displacements (SEDs, between 6 to 77 cm) are interpreted as the result of fault complexity leading to inter-fault dependences and/or the interaction with the latest volcanic activity. Also, small displacements triggered by activity on other faults probably contributed to slip variability, i.e., faults display primary and secondary behavior

Suggested Reviewers: Tom Rockwell
San Diego University
trockwell@mail.sdsu.edu
He already reviewed the paper when submitted to SG

Carolina Canora

Universidad Complutense Madrid
ccanora@geo.ucm.es
She already reviewed the paper when submitted to SG

Jose Miguel Rodriguez-Pascua
Instituto Geológio y Minero de España
ma.rodriguez@igme.es
He knows the study area and have undertaken there several works focused in paleoseismology and geological effects

Departament de Ciències de la Terra i de l'Oceà
Facultat de Ciències de la Terra

Martí i Franquès, s/n
E-08028 Barcelona
Tel. (34) 93 4021376
Fax. (34) 93 402 13 40

10th February 2018

Manuscript for *Geomorphology*

To the Guest Editors, Dr Josep Maria Casas

Dear guest Editors,

Enclosed you will find the reviewed version of the manuscript entitled "**Evidence of recent ruptures in the central faults of the Acambay Graben (Central Mexico)"** María Ortuño, Ona Corominas, Pilar Villamor, Ramón Zúñiga, Pierre Lacan, Gerardo Aguirre, Hector Perea, Petra Štěpančíková and Teresa Ramírez-Herrera, hoping it will be considered for publication in the PATA-days Special Issue. The nature and content of the work presented here have not been published previously and are not under consideration for publication elsewhere.

The manuscript and figures have been prepared in accordance with the guidelines for authors provided on the Geomorphology acta webpage. We hope the paper is found adequate and suitable for publication.

Sincerely,

Dr. María Ortuño Candela

Corresponding author,
maria.ortuno@ub.edu

Department of Earth and Ocean
DynamicsRISKNAT group, University of
Barcelona

Highlights (for review)

Natural outcrops and trenches showed Holocene ruptures in the central faults of Acambay

Six fault ruptures since 12500-11195 BC showed a clustered temporal distribution

Variable single event displacements are considered to reflect complexity of the fault system

Abstract: The Acambay Graben, within the central part of the Trans-Mexican Volcanic Belt, is one of the major sources of continental earthquakes in Mexico. Paleo-earthquake activity is well documented for boundary faults, also source of historic earthquakes. However, the activity and paleoseismological history of the axial faults of the graben are not well constrained so far. We provide morphological, structural and sedimentological evidence for the seismogenic nature of two of the axial structures, the Temascalcingo and the Tepuxtepec fault systems. Faults consist of multiple, parallel, 3- to 25-km-long scarps with *en echelon* and horse-splay patterns. Fault systems extend for 60 km and displace Quaternary to Upper Miocene volcanic materials, fluvial-lacustrine sediments and slope deposits. Observed minimum throws of Upper Miocene and Pliocene markers reach 120-225 m along individual traces. The long-term (0.06 ± 0.02 mm yr^{-1}, minimum) and short-term (0.12 ± 0.02 mm yr^{-1}) slip rate of the Temascalcingo fault system present similar values. Only the long-term slip rate (0.01-0.02 mm yr^{-1}, minimum) of the Tepuxtepec system could be constrained. The Holocene fault rupture history at two sites provided evidence for six ruptures since 12,500-11,195 BC. Three of those ruptures occurred between 11,847 ± 652 BC and 11,425 ± 465 BC. Variable single event displacements (SEDs, between 12 to 87 cm) are interpreted as the result of fault complexity leading to inter-fault dependences and/or the interaction with the latest volcanic activity. Also, small displacements triggered by activity on other faults probably contributed to slip variability, i.e., faults display primary and secondary behavior.

Key words: Temascalcingo fault system; Tepuxtepec fault system; paleoseismology; fault complexity, Trans-Mexican volcanic belt.

Evidence of recent ruptures in the central faults of the Acambay Graben (Central Mexico)

María Ortuño[a,b*], Ona Corominas[a], Pilar Villamor[b], Ramón Zúñiga[c] Pierre Lacan[c], Gerardo Aguirre-Díaz[c], Hector Perea[d,e], Petra Štěpančíková[f], Teresa Ramírez-Herrera[g]

[a] Risknat group. Geomodels Institut. Departament de Dinámica de la Terra i de l'Oceà, Universitat de Barcelona, Martí i Franquès s/n, 08028 Barcelona, Spain

[b] GNS, Institute of Geological and Nuclear Sciences, Lower Hutt 5040, New Zealand

[c] Centro de Geociencias, Universidad Nacional Autónoma de México, Blvd. Juriquilla, 3001, 76230, Juriquilla, Querétaro, Mexico

[d] B-CSI, Department de Geociències Marines, Institut de Ciències del Mar-CSIC, 08003 Barcelona, Spain

[e] GRD, Scripps Institution of Oceanography - University of California San Diego, La Jolla 92093, United States

[f] Department of Neotectonics and Thermochronology, Institute of Rock Structure and Mechanics, Czech Academy of Sciences, V Holešovičkách 41, Praha 8, Czech Republic

[g] Laboratorio Universitario de Geofísica Ambiental, Instituto de Geografía, Universidad Nacional Autónoma de México, Mexico

[*]Corresponding author: Tel. (+ 34) 93 402 13 78; fax: (+34) 93 402 13 40

E-mail address: maria.ortuno@ub.edu

1. Introduction

The highest seismic hazard in Mexico results from large (M $\geq$ 7.5) earthquakes produced by the subduction of the Cocos and Riveras plates under North America along the Pacific margin (e.g., Zúñiga et al., 2017), such as the Michoacán earthquake on September 19th, 1985 (M_w 8.0), which was one of the most destructive events worldwide in the 20th century. Maximum earthquake magnitudes expected from the crustal faults of the Trans-Mexican Volcanic Belt (TMVB) of Mexico are lower (M $\leq$ 7.5) (e.g., Langridge et al., 2000, 2013; Ortuño et al., 2015; Suter, 2016) (Fig. 1). Despite their lower magnitude, these crustal faults are near megacities that have had an exponential increase in their population and urban development during the last decades (e.g., Mexico City and Guadalajara). Therefore, the consequences of fault rupture within the TMVB should not be underestimated, as damage and losses from these events could be quite substantial (e.g., Suter, 2014).

Near 100 active fault traces longer than 2 km have been mapped in the central part of the TMVB (Suter et al., 2001) (Fig. 1). According to their surface expression and age of faulted deposits, many of these have been described as active during the Late Quaternary (Johnson and Harrison, 1989, 1990; Martínez-Reyes and Nieto-Samaniego, 1990; Suter et al., 1992, 1995, 2001; Ramírez-Herrera et al., 1994; Garduño-Monroy et al., 2009). Only nine faults have paleoseismological studies that confirm their seismogenic nature. These are: the Tenango fault, at the eastern section of the TMVB; the Acambay, Pastores, Venta de Bravo, San Mateo and Temascalcingo faults in the central-eastern section (Figs. 1, 2, 3); and the Morelia, Tarímbaro-Álvaro Obregón and La Paloma faults in the central-western section (Langridge et al., 2000, 2013; Norini et al., 2006; Garduño-Monroy et al., 2009; Ortuño et al., 2012, 2015; Velázquez-Bucio et al., 2012; Lacan et al., 2013, 2018, this issue; Sunyé-Puchol et al., 2015; Suter, 2016). Two of these nine faults have been identified as sources of historical earthquakes: the Acambay-Tixmadejé fault, source of the Acambay November 19th, 1912 (M_s = 6.7; Suter et al., 1996; Langridge et al., 2000); and the Venta de Bravo fault, source of the Maravatio February 22nd, 1979 (mb = 5.3; Astiz-Delgado, 1980; Martínez-Reyes and Nieto-Samaniego, 1990). The fact that the seismic potential of other 80 faults with active geomorphic expression is unknown suggests that the seismic hazard of the central TMVB is currently substantially underestimated (Rodríguez-Pérez et al., 2017).

The study of paleo-seismic events from the sedimentary record and the landscape, is one of the most valuable tools to constrain the seismogenic potential of faults. However, within complex systems like the TMVB these studies need to: integrate the characterization of many structures; clarify if they move as primary or secondary faults; and quantify past fault rupture parameters (ie., proxies for future earthquake parameters). In this paper, we focus on the geological and seismogenic characterization of the Temascalcingo-Tepuxtepec-Acambaro (TTA) fault system, a group of faults located along the axis of the Acambay Graben (Fig. 1). To date, the only evidence for Holocene fault rupture within this system was found in a paleoseismological trench across the San Mateo fault (Sunyé-Puchol et al., 2015), antithetic to the Temascalcingo fault (Fig.3A). On the main Temascalcingo fault, Velázquez-Bucio et al. (2012) reported past-fault ruptures observed in trenches, but the work was non-conclusive about the timing of events and their primary/secondary rupture nature.

We present here new data on the TTA fault system from several natural exposures of structural features and five trenches across two of the faults. We used radiocarbon analysis to date displaced sediments. We aim to: elucidate whether these two faults are seismogenic or not; determine a preliminary surface rupture history for each fault; and compare their rupture histories with paleoearthquake chronologies within the region. This latter exercise will help determine the temporal relationship between the axial (TTA) and the larger fault systems bounding the Acambay Graben, i.e., the Acambay and Pastores-Venta de Bravo master faults. Our results will contribute to improving our understanding of the fault activity in the axial part of the graben, and to generating fault sources that can be incorporated into seismic hazard maps and earthquake scenarios of the region. Well constrained hazard estimates are essential for societal earthquake preparedness and response, as well as long term land use planning.

2. Methods

The geology and geomorphology of the central Acambay Graben was studied to mapped fault scarps and assess potential recent fault activity. The method combined the analysis of previously published geological maps (geological maps 1:50000 from the National Institute of Statistics and Geography, INEGI; Aguirre-Díaz et al., 2000, Ferrari et al., 2012; Ortuño et al., 2015) with the study of landforms. We undertook aerial photograph interpretation (1:37000 scale flight from 1983 available form INEGI), analysis of digital elevation models (obtained from 1:25000 digital topography available from INEGI) and field reconnaissance. We compiled structural data (including kinematic indicators) at eight natural outcrops associated with fault scarps to determine fault geometry and kinematics. We also documented the characteristics and potential age of faulted volcanic and fluvial deposits at the natural exposures.

Based on presence of potential surface deformation from geomorphic analysis, and observations from nearby artificial and natural outcrops, sites were selected for detailed studies along the Temascalcingo and Tepuxtepec fault systems (Fig. 1). The selected trench sites were located on Holocene to Late Pleistocene sediments and had potential for containing datable material. During April 2011, paleoseismological trenches were excavated with a backhoe excavator and were perpendicular to inferred fault traces on both fault systems. The excavation was between 10 and 18 m long and 2 m wide with vertical walls of approximately 2.5 m depth. Trench walls were gridded (1 m x 0.5 m) and logged at a 1:20 scale. Photomosaics of the trench walls are available as supplementary material (A.1 and A.2).

The analysis of the structure and stratigraphy exposed in the trench walls, aided with retro-deformation of the logs, allowed for the determination of the number and characteristics of the rupturing events. We provide estimates for vertical slip-per-event, and then calculated the dip-slip per event using the dip of the major fault. These measurements have associated uncertainties derived from two main sources. The first and larger uncertainty is related to the use of alternative markers to calculate the fault throw. For instance, the basal surface of some units is irregular but can be simplified with a straight line (envelope) that can be subjectively delineated in different ways. In those cases, two envelopes, representing maximum and minimum displacements, have been considered and used to calculate an average value and its associated error (Supp. Mat A.3). The second uncertainty is based on the repeated measure of the associated displacements, which led us to detect an extra systematic error of: near ± 2 cm for trench data, i.e., derived from transferring the lines from the trench wall to the log and from log digitalization; and of ± 10 m for geomorphic surface throw, derived from digital elevation model resolution. The uncertainty in the offset calculations combines both errors considering a uniform distribution.

To constrain the timing of deformation, 10 samples of charcoal and soil were collected and dated. A chronological model of the rupturing events in Juanacatlan site was obtained considering the probability distribution of ^{14}C dating results. This was done following the procedure proposed by Lienkaemper and Bronk Ramsey (2009) for the Bayesian treatment of the dating results with the OxCal program (version 4.2; Bronk Ramsey, 1995, 2001, 2008).

3. Geological and seismotectonic setting

The central part of continental Mexico is traversed by the TMVB, an active volcanic arc that extends from the Pacific to the Gulf of Mexico for nearly 1000 km (Fig. 1). The emplacement of this arc during the Neogene is associated to the subduction of the Cocos and Rivera plates under the North America plate (e.g., Mooser, 1972; De la Fuente and Verma, 1993; Ferrari et al., 2012). The study area is located within the central part of the TMVB, also known as the Chapala-Tula fracture zone (Johnson and Harrison, 1990). Since the middle Quaternary, the minor horizontal stress vector (σ_3) for central TMVB is oriented northwest-southeast (Suter et al., 1995, 2001; Ego and Ansan, 2002), with an accumulated bulk extension rate across the volcanic belt of 0.2 ± 0.05 mm yr^{-1} (Langridge et al., 2000; Suter et al., 2001).

The Acambay Graben is one of the east-west oriented grabens within the central TMVB (Aguirre-Díaz, 1996; Fig. 1). This graben is bounded by four major faults, the Acambay-Tixmadejé and Epitacio-Huerta faults to the north and the Pastores and Venta de Bravo faults to the south. The graben widens towards the west in a scissorslike pattern (Fig. 1). The first active faulting studies focused on the faults bounding the Acambay Graben (e.g., Martínez Reyes and Nieto-Samaniego, 1990; Ramírez-Herrera et al., 1994; Suter et al., 1995, 2001). During the last two decades, the research has focused on characterizing the seismogenic potential and the paleoseismic history of the Acambay, Pastores, San Mateo and Venta de Bravo faults (Langridge 2000; 2013; Ortuño et al., 2012; 2015; Velázquez-Bucio et al., 2012; Lacan et al., 2013; 2018, this issue; Sunyé-Puchol et al., 2015). According to those studies, these faults could generate earthquakes of maximum magnitude (M_w) between 6 and 7, with recurrence intervals between 3.6 and 14 kyr (Langridge et al., 2000, 2013; Sunyé-Puchol et al., 2015). Ortuño et al. (2015) inferred shorter recurrence intervals (1.1–2.6 ka) for the western tip of the Pastores fault, and suggested that the fault segment, located in a transfer zone, could have recorded secondary ruptures associated with large earthquakes on nearby faults.

3.1 The Acambay central faults

The ESE-WNW to E-W trending Temascalcingo-Tepuxtepec-Acámbaro (TTA) fault system (Martínez-Reyes and Nieto-Samaniego, 1990) consists of a set of faults that extends for approximately 100 km between Temascalcingo and Acámbaro (Fig. 1). It can be divided along strike into three fault subsystems, the Temascalcingo (eastern part), the Tepuxtepec (central part) and the Acámbaro (western part) fault subsystems. While the Temascalcingo and Tepuxtepec subsystems are located within the Acambay Graben, the Acámbaro subsystem is located outside the graben. Most of the faults in the Temascalcingo and Tepuxtepec subsystems dip to the north, whilst in the Acámbaro faults dip mainly to the south. Minor faults within these subsystems define several tectonic basins, such as the San Antonio-San Rafael basin, or the one located at the top of the Temascalcingo volcano (Figs. 1, 2, 3). The Altamirano volcano appears to be the boundary between the Temascalcingo and Tepuxtepec faults systems.

Although not described thoroughly, the recent activity of the TTA system has been highlighted in previous regional studies. Fault activity was inferred from geomorphological expression and from analysis of outcrops, where fault planes and slicken-lines were found on rocks older than middle Quaternary (Martínez-Reyes and Nieto-Samaniego, 1990; Ramírez-Herrera et al., 1994; Ramírez-Herrera, 1996; Suter et al., 2001). Preliminary paleoseismological data on these faults were presented by Ortuño et al. (2011).

4. Late Pleistocene and Holocene activity of the Temascalcingo-Tepuxtepec system

More than 20 faults traces have been mapped within the Temascalcingo and the Tepuxtepec fault subsystems (Fig. 1) Many of the faults displace three major volcanic complexes. These are, from east to west, the Temascalcingo volcano, the Altamirano volcano, and the Puruagua volcanic range (Aguirre-Díaz, 1996). The two former ones are Quaternary andesitic-dacitic strato-volcanoes and the latter is a Miocene volcanic complex (Aguirre-Díaz et al., 2015; Fig. 1).

4.1 The Temascalcingo fault system

The N100-110ºE trending Temascalcingo fault system (TemasFS) extends for 32 km from the Acambay valley (east of the Temascalcingo volcano) to the eastern foot of the Altamirano volcano. The fault system comprises 10 distinctive faults and displays two contiguous horse-tail geometries that open to the east (Fig. 3A). The separation perpendicular to fault strike between the fault traces has a maximum value of 6 km near the centre of the Temascalcingo volcano. Splaying fault terminations have been observed in other parts of the Acambay Graben, such as with the Venta de Bravo fault and the western end of the Pastores fault (e.g., Suter et al., 1992; Ramírez-Herrera, 1998; Ortuño et al., 2015; Lacan et al., 2018, this issue; Fig. 1).

The main geologic and geomorphic units displaced by the Temascalcingo fault subsystem (Fig. 3A, Supp. Mat. A.4) are, from east to west (Sánchez-Rubio, 1984; Aguirre-Díaz, 1996; Aguirre-Díaz et al., 2000; Roldan-Quintana et al., 2011; Ortuño et al., 2015; Pedrazzi et al., 2016): **1**) the Plio-Quaternary Santa Lucia dacitic dome (TQsld in Supp. Mat. A.4); **2**) the Temascalcingo dacitic-strato volcano of Quaternary age (Aguirre-Díaz et al., 2015); and **3**) the Pliocene Bañí dacitic domes. In the eastern sector of the TemasFS, the Temascalcingo volcano is vertically offset by north dipping and by south dipping faults along its southern and northern flanks, respectively. This faulting has resulted in the formation of counter-slope scarps, associated basins and drainage blockage, and the modification of the volcanic summit caldera (Figs. 2aA, 3A). In the western sector, the Bañí-Solís domes (with mesa-type reliefs) are offset by north dipping faults, which have led to a stair-case like landscape (Figs. 2aB, 2aC, 3A, 4).

4.1.1 The Temascalcingo fault surface expression

The Temascalcingo fault is the main fault within the TemasFS. It dips near 80º to the north, has a length of 19 km, and comprises three segments according to its surface expression (TF1 to TF3 in Fig. 3A). The 10.6-km-long eastern segment (TF1) bounds the San Pedro caldera to the south. TF1 connects and overlaps by 2 km with the central segment of the fault (TF2) near the Lerma River. The straightness and continuity of both segments suggest that they are linked at depth. The 7.3-km-long TF2 segment cuts across the mesa reliefs formed by the Bañí-Solís domes. These tabular reliefs dip gently to the south as a result of tectonic tilting (Figs. 2C**,** 3A). The western tip of TF2 cuts a well-preserved cinder cone. The 6.1-km-long western segment (TF3) extends from the Bañí-Solís domes to the eastern flank of the Altamirano volcano (Fig. 3A). To the north, TF3 connects with two ENE-WSW trending fault branches that form the western horse-tail of the TemasFS. Four fault outcrops (Table 1, Figs. 1, 5) along the Temascalcingo fault segments showed predominantly normal faulting of late Quaternary volcanic materials.

4.1.2 Paleoseismological exposures of Temascalcingo fault (Juanacatlan site)

At the western end of the TF2, the Juanacatlan trench site (Figs. 3A, 6) was selected for paleoseismological investigations. The site is located at a hydrological divide defined by the Altamirano and Temaslcancingo volcanoes, that separates the the Lerma River valley to the north from a local Quaternary fluvio-lacustrine basin to the south. The site is local at topographic low along the divide where he local morphology appears that of a smooth valley between two volcanic reliefs (the lava domes to the East and a cinder cone to the west). At this location, talus deposits accumulate. This site, along the trace of the major TF2, was suitable for paleoseismology studies because of: **1**) its proximity to structural station 1 (Fig.1, Table 1), which provides structural data for the TF2 indicating active normal faulting affecting a Quaternary cinder cone (El Ruedo, Figs. 3A, 5A); and **2**) the presence of relatively low (<2 m high), easy-to-trench scarp, considered favorable for the preservation of the same sedimentary units on both sides of the fault. We assumed that a balanced relationship between deposition and erosion has allowed for a better recording of the faulting history here, compared to surrounding areas. The drainage to the south has limited erosive capacity, as the topography (now occupied by the Juanacatlan Lake) is relatively flat.

At the Juanacatlan site, two 3-m-deep, 10-m-long trenches (Juana 1 and Juana 2) were excavated across the fault and were10 m apart (Fig. 6). Seven samples for ^{14}C dating were collected (Table 2, Fig. 6). Juana 1 exposed a volcano-sedimentary sequence consisting of nine units named *a* to *i* from younger to older (Fig. 6). The sedimentary unit properties are described in Supplementary Material A.4 and have been used to interpret the origin of the units provided below and included in the figures containing the trench logs. At the base of the trench, an ignimbrite deposit (unit *i*) is buried by two sedimentary units: a reworked regolith (unit *h*) and a channel infill (unit *g*). Unit g is only present next to the main fault and it is a matrix-supported conglomerate with rounded dacite and ignimbrite clasts up to 14 cm diameter. The roundness of the clasts leads us to interpret it as a fluvial unit filling, a channel running parallel to the fault scarp. Units *h* and *g* are only present in the hanging-wall. Unit *f* is a paleosol with colluvial clasts and pedogenic calcite laminae. It overlays units *h* and *g* in the hanging-wall and unit *i* in the footwall. On the west trench wall, a colluvial deposit is juxtaposed to the main fault and is interpreted as a colluvial wedge (unit *e*). A sequence of weathered air-fall deposits (ash and clay deposits; units *d*, *c* and *b*) formed the upper most part of the depositional sequence. The topmost layer is the present-day soil that is disrupted by ploughing. Faulting was distributed across a main fault and secondary synthetic and antithetic faults (up to 11 faults and fractures). Secondary faults mainly developed within the down-thrown block. The main fault is oriented N114E to N124E, dips 65N and displaces all the volcano-sedimentary sequence except for unit *b* that is only fractured, and unit *a* that is undeformed. The accumulated vertical displacement of unit *h* is 1.39 ± 0.14 m (Juana 1E) and 1.85 ± 0.17 m (Juana 1W).

Juana 2 (Fig. 6) exposed the same volcano-sedimentary sequence in the downthrown block as in Juana 1, whereas in the upthrow block it only exposed a dacitic lava-flow (unit *j*) covered by unit *a*. Unit *j* belongs to the Bañí-Solís domes (Fig. 3A). We did not identify units *g*, *f'*, *f* and *e* in this trench. Faulting is displayed as a main N114-120E trending fault and a series of synthetic and antithetic faults. One of the secondary fault planes developed in unit *j* oriented N095-099E/85N exhibited slickenlines 43/105, indicating a main dip-slip fault with a minor right lateral component. It is notable that the fractured/faulted zone becomes wider to the west (Juana 2-W), and that there is a preferentially depressed area located in the downthrown wall. This zone is bounded by faults and it can be identified in all the trench walls. The cumulated vertical displacement of unit *h* has been estimated as 1.71 ± 0.26 m (Juana 2E) and 1.56 ± 0.3 m (Juana 2W).

4.1.3 Paleoarthquake sequence at Juanacatlan site

Analysis of deformation in the two trenches at the Juanacatlan site suggests a sequence of at least six surface ruptures with variable single event displacement (SED) ranging from 6 to 77 cm (averaged in 46 ± 6 cm), with a coefficient of variation of 0.46 (vertical component). The style of deformation varies from one trench to another, and some events cannot be identified in all of them (Fig. 6). While the styles of deformation in Juana 1 and Juana 2E are similar, with most of the deformation localized on a main fault, Juana 2W displayed a very different style. In this latter, faulting seems to be somewhat more broadly distributed and having larger offsets along some faults in association with fissuring. We interpret that Juana 2W deformation style is highly influenced by voids developed in the near surface along the fault, which causes collapse of blocks between faults, and thus large fault throws that may not representative of the tectonic displacement. Consequently, while we have reported the apparent displacements observed in this trench, we have not considered them as preferred in any case.

The faulting history was deciphered by step-wise restoration of two trench walls of Juana 1E (Fig. 7) and by analyzing the geometric relationships between faults and sedimentary units, as well as progressive displacement, in the four trench walls (summarized in Table 3, Supp. Mat. A.5, A.6). Fault ruptures are interpreted to have produced folding and simultaneous displacement on several fault branches. In Table 3, we provide the throws associated to faults active during each event, but only to show relative timing the ruptures. Collapse of the fault free face is recorded as a colluvial wedge (in Juana 1E) and at least in one occasion, the generated scarp may not have been completely eroded between successive ruptures.

Event 1. The bracketing units for event 1 are *a* and *b*. The most recent surface rupturing event produced displacement along two of the faults observed at Juana 2W, and tilting and fractures along different zones in both trenches. Main evidence for this event is movement of F5’, the main fault at Juana and a fissure opening along F10’. Deformation along F8’seems to have caused the down-drop of unit *b*. At Juana 2E, Juana 1E and W, this event is less obvious. It probably displaced the base of unit *c* by 57 ± 3 cm. At Juana 1W, displacement and tilting of unit *b* along the main fault is considered as feasible, but the exact amount of deformation produced by this event cannot be distinguished from the deformation during event 2. Also, some inherited throw is suspected.

Event 2. Rupturing event 2 was inferred from the deformation of unit *c*, which does not extend into unit *b*. It has an associated SED ranging from 78 ± 17 cm to 60 ± 3 cm, inferred from the displacement of the base of unit *c* in Juana 1E and Juana 2E. Evidence for this event in Juana 2E is that unit *c* seals the main fault but it is displaced by other faults. The increased thickness of unit c in the area bounded by faults F2 and F8 (at Juana 2E) and F4' and F8' (at Juana 2W) is considered the most striking evidence of this event. F2 cuts unit *c* which is bounded by two fractures interpreted as a tectonic fissure. At Juana 2W, this deformation is expressed by relatively large offsets of unit *c* and underlying units across faults F4' to F12'.

At Juana 1W, the measured throw (75 ± 10 cm) could include some inherited throw from a previous event, since the presence of a scarp leading to a colluvial wedge (in next event) suggest that the top of unit *d* was never completely horizontal. This inheritance could also be present in the measured values of the other trench walls but the absence of a colluvial wedge does not allow for its estimation.

Events 3 and 4. Two previous events are identified by the larger deformation of unit *d* with respect to younger units (event 3) and by the formation of a colluvial wedge (unit *e*) on top of unit *f* (event 4). We analyzed the deformation of these two events together (events 3/4) because unit *f* is not present in Juana 2 and, thus, both events appear as single event.

Event 3 is bracketed between units *c* and *d*. The main pieces of evidence for this event are: **1**) the sealing of some faults and fractures by unit *c* (F10 in Juana 1E; F5' to F6'in Juana1W; F5 in Juana 2E; F9' in Juana 2W); and **2)** the fact that the colluvial wedge (unit *e*), generated in previous event (event 4), is faulted. The measurement of its associated SED (discussed below) was not straightforward; we suspected that unit *d* may have not been horizontal prior to faulting by event 3. Therefore, to determine its

SED we required first to estimate the “inherited throw”, i.e., the displacement produced by the prior event.

Event 4 is bracketed between units *d* and *f*. In Juana 1W, the main evidence for event 4 comes from the presence of a colluvial wedge (unit *e*) between the two bracketing units next to the main fault. Unit *e* consists of irregular and angular clasts derived from units *f* and *j*. It has an associated SED of ~80 ± 6 cm and 80 cm ± 8 cm, measured at Juana 1E and W, respectively. The first value is inferred by multiplying the thickness of the colluvial wedge (unit *g*, 53 ± 4 cm) by 1.5 times, which result in value similar to the displacement of unit d in Juana2E and is in the range of the estimations made by McCalpin (2009) from observed relationships between colluvial wedges and source scarp.

In Juana 2E and W, we cannot distinguish between events 3 and 4. The cumulative displacement of unit *f* of 30 ± 15 cm represented the combined SED. Restoration of these events is difficult because we suspect that, before event 3, unit *d* (ash fall deposit) was not horizontal but had a depositional geometry that mimics a scarp (Fig. 7), indicating that between event 3 and 4, the ground surface was not completely leveled. Moreover, the thickening of unit d in the fault zone also suggests it was burying a step in the ground (preexisting scarp). This is consistent with a fall deposit mantling the surface scarp produced during event 4. This configuration can be compared with that observed at paleoseismological trenches across fault in volcanic environments (e.g., the Rangipo fault, in the Taupo volcanic rift, New Zealand; Villamor et al., 2007), where volcanic tephra deposits mantled pre-existing surface scarps, inheriting the surface offset.

Event 5. The event 5 is constrained between units *f* and *g* in Juana 1 and between units *d* and *h* in Juana 2. In Juana 1E, several faults and fractures cut unit *g* but not unit *f* (meters 4 to 5 in Fig. 6). For some of these structures (e.g., F6 to F8) it is not possible to distinguish if the base of unit *g* is displaced or just fractured because the base of the unit is not exposed. In Juana 2W, the deformation assigned to this event is distributed among several fault branches. There, the base of unit *h* is clearly more displaced than the base of unit *d* (for instance, along F2', F3', F10'to F12'). The absence of unit *h* between faults F7' and F8' suggests that some erosion took place right after deposition of unit *h*, which is consistent with the formation of the channel infill observed at Juana 1 (unit *g*). The area between faults F5' and F10'in Juana 2W is interpreted as a small graben developed within the downthrown wall (meters 4 to 6 in Fig. 6), with some large fault displacements enhanced by vertical collapse of the units (subsurface voids). A similar structure is identified at Juana 2E between F3 and F8.

The cumulative throw (CT) of event 5 in the different trenches is obtained by assuming that the base of unit *h* on the downthrow block was at some time leveled with the top of unit *i* in Juana 1 (Fig. 7) and of the top of unit *j* in Juana 2, both on the upthrown block. This value should be considered a minimum, because some erosion on the upthrown block might have occurred. The CT ranges between 139 ± 14 cm (Juana 1E) and 185 ± 17 cm (Juana 1W). After subtracting previous events from these values, the preferred SEDs of event 5 are 32 ± 5 cm (Juana1E) and 56 ± 3 cm (Juana2E).

Event 6. This is the oldest identified event and is characterized by deformation on unit *i* that is not present in unit *h*. In Juana 2E, such a deformation is obvious along faults F2, which are filled with material from unit *h*, F3 and F7. The differences in weathering degree between the top of unit *i* in the hanging wall and in the footwall (observed in Juana 1E and 1W trenches) hampers correlating theses markers across the main fault. Accordingly, the throw obtained by leveling these two surfaces must be considered as a minimum, because the “weathered” top of unit *i* in the upthrown block could have been at a higher elevation and subsequently been eroded. For Juana 2E and 2W, we have assumed that the top of unit *i* was at some time leveled with the top of unit *j*. Therefore, the total cumulative throw calculated at Juana 2E is 228 ± 25 cm (64 cm SED), which should be taken as a minimum offset.

4.2 The Tepuxtepec fault system

The E-W trending, mainly N dipping Tepuxtepec fault system (TpFS) is located between the Altamirano volcano and the western slopes of the Puruagua Range. It displaces the volcano flanks, and the Lerma River fluvial depression at two locations (Fig. 1). The TpFS comprises a total of 16 faults with lengths ranging between 1 and 18 km and maximum scarp-heights between 15 and 125 m. Three main faults (Figs. 1, 3B) are defined from fault trace geometry as (1) the Taranda (22 km long) fault, (2) the Paquisihuato North (PNF in Fig. 1; 8 km long) and South (PSF in Fig. 1; 7 km long) faults, and (3) the Tepuxtepec (25 km long) fault. The E-W trending Taranda fault is the northernmost fault of the system and dips to the N (Figs. 1, 2bE), while Paquisihuato South fault bounds the system to the south. The E-W to ENE-WSW trending Tepuxtepec fault shows a sinuous trace, a dip to the N (Fig. 2bF), and splits into several fault traces at the eastern end. Some of those traces displace the Altamirano volcano (Fig. 3B).

Most of the fault traces separate hard lavas (uplifted blocks) from areas with accumulation of volcano-sedimentary sequences (downthrown blocks, Fig. 3B). From older to younger, the principal volcanic sequences are: **1)** the Sierra Puruagua complex, a Miocene volcano-sedimentary sequence (Aguirre-Díaz et al., 2012; Ortuño et al., 2015) that mainly consists of lavas and pyroclastic flows; **2)** pyroclastic fall deposits and flows of undefined age, mainly preserved in the downthrown block; **3)** a Pleistocene pyroclastic fall (Aguirre-Díaz et al., 2015) covering a wide area and exposed at the eastern sector in several quarries (station 4 and 5 in Table 1 and Fig. 1, Supp. Mat._ A.4).

The geomorphological expression of the Tepuxtepec faults analyzed with respect to the distribution of the lithologies and the drainage pattern (Fig. 1 and 3B, Supplementary material A.3 and A.8) allows for a preliminary evaluation of the degree of activity of the system. The activity of faults clearly controls the current drainage pattern. The drainage delineates a typical right-angle cross pattern with fluvial courses running parallel and perpendicular to the faults. Fluvial depressions have elongated shapes and run parallel to tectonic structures (subsided areas), such as the San Antonio-San Rafael graben (Fig. 3B). Creeks flow parallel to faults (within the elongated depressions) and at the base of large fault scarps (drainage parallel to faults, Fig. 1, 2D-F, Supplementary material A.8).

Ramirez-Herrera (1994; 1998) suggested that the activity of the Tepuxtepec fault system, inferred from scarp dissection and triangular facets analyses, was relatively low compared to other systems within the Acambay graben. While this is possible, there are other factors, such as lithology, size of drainage basins and fault geometry, that may hinder scarp dissection and/or formation of triangular facets even if the activity of faults is moderate or high (Wells et al., 1988). The regional relief at the southern flank of the Puruagua range is relatively low and controlled by successions of Miocene lava flows. This low relief combined with resistant lithologies might have hampered the incision of fluvial drainage perpendicular to the fault scarps (Fig. 3B, Supp. Mat. A.3 and A.8). Accordingly, the poor faceting of the fault scarps might not be indicative of relatively lower tectonic rates. Moreover, the faults present relatively shorter lengths when compared with the other fault systems in the region (Fig. 1). A low degree of fault linkage might be indicative of the early stage of fault systems compared to longer and supposedly older fault systems (e.g., Dawers and Anders, 1995; Roberts et al., 2004). In the study area, faults within the axis of the graben (Tepuxtepec area) could be thus younger but not less active than faults bounding the graben (as Acambay-Tixmadejé fault), where fault segments are longer (Fig. 1). The recent linkage between segments can also be suspected from the scarp height distribution. The topographic profile of the upper and lower part of the scarp along the main fault trace (TpxF1) shows two sections of increased throw and another section with smaller throw in the middle. This feature suggests that the fault may have resulted from the recent linkage of two consecutive segments, showing a lower throw in the middle part of the trace (Fig. 4B). However, we agree with Ramirez-Herrera (1998) that the morphometric analysis of faulting in this area is problematic because: of lithological control on the scarp morphology; the system does not represent a continuous mountain front; and the geomorphology also reflects volcanic processes.

4.2.1. The Tepuxtepec fault surface expression

The 24-km-long Tepuxtepec fault (TpxF) is the largest fault within the TpFS. It extends from the western slopes of the Altamirano volcano to the west of the Puruagua range. The system consists of multiple fault segments displaying horse-tail like geometry (Fig. 1). A main fault displays relatively large surface offsets with a maximum thrown of 125 m (Fig. 4B). Secondary faults tend to concentrate in the upthrown block and show lower scarp heights (between 15 and 55 m).

The TpxF can be divided into two segments, the 3.5 km long TpxF1 and the 4.5 km long TpxF2 (Fig. 3B). In the TpxF1 footwall, two parallel faults, the San Rafael (~ 7 km long) and San Antonio (6.4 km long) faults, define a tectonic graben filled with fluvio-lacustrine sediments. Within the San Antonio-San Rafael graben, the *Cerro Prieto* dome seems to be tectonically displaced by small faults. To the west, the *Cerro Pelón*, a cinder cone of probable Quaternary age, is displaced by the San Rafael fault (Fig. 3B).

The geomorphologic expression of the TpxF corresponds mainly to normal faults. Topographic profiles across the TpxF (Fig. 4B) suggest that most of the faults dip to the north, except for the San Antonio fault, that dips to the south. The height of the escarpment, up to 50 m, increases towards the center of the faults.

Five structural outcrops along the Tepuxtepec faults (located in Figs. 1) confirmed the Late Quaternary fault activity and its predominant normal component of displacement (Table 1, Fig. 5). Structural data collected at these stations suggest that the regional extension direction is approximately NW-SE.

4.2.2. Paleoseismological exposures at San Antonio fault

Three trenches (Tepux 1, Tepux 2 and Tepux 3) were excavated across the E-W trending, south dipping San Antonio fault (Figs. 1, 3B). The trenches are located near the central part of the fault trace. In this area, the scarp is developed on dacitic lavas of probable Pliocene age, and the area is now partially urbanized. The site was chosen because the scarp is smaller here (5-10 m high) than that along the rest of the trace (15-20 m high). Unfortunately, the presence of a frequently used gravel road between trenches 1 and 2 didn’t allow us excavating a trench at the location we predicted the major hypothetical fault branches to be located.

The trenches were excavated in a direction perpendicular to the fault and were 2.5 - 3 m deep and 10 to 18 m long. We only provide the logs of the western walls except for the section with the fault zone, observed in Tepux 2, for which both walls were analyzed. Sedimentary units s are described in Supplementary Material A.4, and have been used to interpret the origin of the units provided below (Fig. 8).

In Tepux 1 the three sedimentary units were identified, from bottom to top, a flood deposit (unit *e*), a slope deposit (unit *w*) and the present-day soil (reworked by ploughing). In Tepux 2 and Tepux 3, there is an alternation of flood plain and volcanic ash fall deposits (all units in trench 2 and 3, with the exception of unit *b1*). In Tepux 2 and below unit *e*, units *f* and *g* are interpreted as a flood deposit with reworked ash, and as a fluvial channel infill of medium-low energy, respectively. At the southern end of Tepux 3, unit *b1* appears as a fluvial channel infill deposit. Many of the exposed units have an associated paleosol. The fluvial units are interpreted as the record of a paleo-river draining from east to west, connecting the sub-basins east and west of the *Cerro Prieto* hill (Fig. 3B). At present, the river is relatively small (a seasonal creek) and it is incised in the fluvial sediments from the prior larger river.

The age and characteristics of the sedimentary units (Table 2, Supp. Mat. A.4) and their location on the slope allowed for the correlation of units between trenches. We also relied on a microtopographic profile (Fig. 8 upper inset) and in a Ground Penetrating Radar profile (included in Corominas, 2011) to correlate the units between trenches. For instance, it was possible to identify unit *e* in Tepux 1 and Tepux 2 and, thus, we interpret that overlying unit *w* (Tepux 1) changes laterally to units *b*, *c* and *d* (Tepux 2).

The deformation in these trenches is relatively small, and it is only evident in Tepux 2 (Figs. 2aC, 2bD). Evidence for the tectonic nature of the exposed features (Fig. 8) is described next. (**1**) The 12º dip of units *a* to *e* is interpreted as tectonic tilting. These units are the infill of a fluvial plain of a river running from E to W, perpendicular to the trench. Their original geometry is expected to be sub-horizontal in the cross section of the trench. Such a tilt may have been caused by one or two major faults not exposed in the trenches. (**2**) In Tepux 2E, units *f* to *c* are faulted by a set of six N095E trending, subparallel fault branches that likely merge into two faults at depth. F1-3 may merge into a main fault and F4-6 into another. Each of these faults have associated displacements that range between 2 and 14 cm. **3**) Additionally, in meters 2-3 of Tepux 2E, we detected two blocks of material involved in the fault zone (fault-bounded), referred to as a "mixed unit" (unit *e'*). These are made of a mixture of sediments from unit *e* and *d*, suggesting the seismogenic nature of the deformation.

The fault kinematics could not be clearly inferred from the trench exposures, where no fault planes or slicken-lines could be measured. Although we do not have solid evidence, we think that the main fault (MF1, Fig. 7) control the surface expression of the TpxF and may be situated at some depth below the surface scarp. The MF1, inferred between trenches 1 and 2, may result in a fold scarp on the surface (Fig. 8 upper inset). If correct, the surface scarp could be the result of an accommodation of younger units that mimic the tectonic scarp or the result of a flexural fold scarp. Alternatively, the main fault may reach the surface along the road, where excavation was not permitted. The small displacements observed at the exposed faults are interpreted as antithetic branches of the MF1. Fault geometry of F1 to F6 shows bifurcations and relays that suggest that the faults are strands of a main fault with some lateral movement. Accordingly, fault vertical displacements reported might be only apparent. This is also supported by the changes in the thickness of the units observed across some faults (F3, F5-6). F4 cannot be clearly traced into unit *d*, which could be explained as related to lateral fault termination.

An estimate of the recent vertical slip accommodated by the hypothetical fault causing the fold scarp was done by considering the offset of unit *e* as it has been connected in the log of Fig. 8, which is 1.18 m ± 0.1 m.

4.2.3. Paleoearthquake sequence of San Antonio site

From the analysis of deformation in the trenches (mainly in Tepux 2), we infer the occurrence of two surface rupturing events.

Event 1. The youngest event occurred after deposition of unit *c* and is evidenced by displacement of units *c* and underlying units along all faults except for F4. This event produced mixing of units, observed at the fault-bounded blocks (unit e').

The vertical displacement of unit *c* along faults F1, F2 and F3 is less than 12 cm. The movement along F5 and F6 faults has created an 8 - 9 cm apparent offset at the base of unit *c*. The suspected fault between trenches 1 and 2 (Fig. 8), which deforms unit *c* and underlying units, might have been active during this event, causing the downthrown movement of the southern block.

Event 2. Evidence of the penultimate event exposed in the trench 2 is weak. It should have occurred after unit *e* and before unit *d*. Evidence is only based on the faults F1 and F2 displacing unit *e* and underlying units, as seen in trench 1. This displacement is also small, between 10 and 15 cm.

5. Chronology of surface ruptures

Integrating the trenching analysis of the two sites (Juanatlan and Tepuxtepec) and the ages of the units obtained from radiocarbon dates (Table 2), we propose a chronology for the surface rupture events. Samples taken for ^{14}C analysis yielded conventional radiocarbon ages between 15,370 +320/-310 kyr BP and 4195 +/-95 kyr BP in Juanacatlan trenches, and between 11,950 +/-160 kyr BP and 3491 +/-44 kyr BP in Tepuxtepec trenches (Fig. 6, 8, Table 2). Among the 10 samples dated, four of them (JUA 2-1, JUA 2-3, JUA 2-6, T2-16F) are not consistent with the stratigraphic order and have been considered outliers. For Juanacatlan trenches, samples JUA 2-1 and JUA 2-6 come from unit *d*, interpreted as an ash deposit. It is likely that the recycling of old charcoal could provide an older age than that of the sediment. Accordingly, this samples have not been considered in the chronological model. Also, JUA 2-3 sample (taken in unit *h*) has been excluded because it is considered anomalously young (1220-815 BC). We think that this relatively young age might be related to some edaphic (leaching) process affecting the re-worked ignimbrite and rejuvenating it. For Tepuxtepec, sample T2-16F is not considered representative of depositional age. It is as bulk sample collected from a flood deposit, which may have incorporated older material.

Thus, only four samples for Juanacatlan and two samples for Tepuxtepec sites have been incorporated in the chronological model (JUA -7, JUA 2-5, JUA 1-FG-1, JUA 1-1, TEPUX 3.7, TEPUX-2; Fig. 9; Oxcal files provided in the Supp. Mat. A.7). For both trench sites, the beginning of 20th century has been considered as an upper boundary for the occurrence of rupturing event 1. The year 1700 in Central Mexico can be considered as a reference starting time for a sufficiently complete historical and instrumental catalogue (Gerardo Suárez, per. com.). Because no seismic events with intensities > VII-VII are reported in the area since that time, 1700 has been taken as an upper boundary for the occurrence of event 1 in Juanacatlan.

In the Juanacatlan sequence, the paleo-ruptures of events 3, 4 and 5 are treated in the OxCal analysis as a multiple event because no valid age result is available to better constrain the events. Accordingly, Event 1 occurred more probably between 2565 BC and 1900 AD. Event 2 is very roughly constrained and should have happened at some time between 11,030 and 2871 BC. Considering the large time span non-recorded in the trench and the relatively large SED assigned to event 2 (as high as 75 ± 11 cm in Juana1E), a possible double event is considered as feasible. Events 3, 4 and 5 are clustered between 11,847 ± 652 BC and 11,425 ± 465 BC. This implies a maximum time span of 1720 yrs for the occurrence of these tree events. Event 6 should have occurred before deposition of unit *h*, this is, sometime before 12,500-11,195 BC.

The age distribution of the events recorded in Juanacatlan site suggests a non-periodic behavior of the Temascalcingo segment (TF2). The most striking result is the clustering of 3 surface ruptures (events 3 to 5, Fig. 9) within maximum time span of 1443 years. These results need be considered preliminary for two reasons. The first reason is that the assumptions made for the analysis of the number of events creates large uncertainties. The lack of a high-resolution sedimentary record could lead to interpret multiple surface ruptures as a single one. For instance, there is an almost 10 kyr difference between units *b* and *c* which bracket event 2 (Fig. 9). In those cases, the size of the SED associated with this event has been critical to decide on the number of events. This is, if a certain event corresponds to the record of a single or a multiple event. The second reason is there are not enough radiocarbon dates to create a robust OxCal model. In fact, the consideration of sample Jua-2-1 (unit *d*) as a “preferred age” in front of samples Jua-1-FG-1 and Jua 1-1 (unit *g*) would produce an alternative valid model. In such a model, the distribution of earthquakes would change slightly (maximum boundary for events 3, 4 and 5 would be 13,525 BC and not 11,939 BC). This would lead to an extension of the clustering time span from 1443 years to 2468 years.

The chronology of paleo-ruptures in Tepuxtepec site can only be roughly estimated, because only two dating samples are considered consistent. Accordingly, we only can constrain the two observed events as occurring between unit *e* and unit *b1*. Because of the scarcity in number of samples, we have considered a single calibration of the two valid samples (Table 2). Event T1 happened at some time between 3515-3105 BC and 2570 - 2295 BC, and Event T2, shortly after a time in the range of 3515 – 3105 BC. This constrain implies a cluster of two events in a time range of 1220 – 535 years.

6. Faulting style and fault slip rates

Fault exposures confirm that the morphological features mapped are indeed the expression of active and seismogenic faults displacing Quaternary materials. The main component of movement is dip slip based on kinematic observations in outcrops and trenches, and from geomorphic analysis. In other natural and trench exposures in the Acambay Graben, primary normal faulting is also observed when the main fault trend is meridional. However, in fault sections with NNE-SSW or NNW-SSE trends (departing from the most common strike of the systems) (some left and right components are also reported. For instance, this is the case of the trench exposures studied at the eastern end of the Acambay fault by Langridge et al. (2000). The structural data compiled here (Fig. 5) are consistent with a minimum horizontal stress (σ3) oriented NW-SE to N-S, which is also reported in more representative studies analyzing larger datasets (e.g., Suter et al., 1995, 2001; Ego and Ansan, 2002).

The long-term (late Miocene or Pliocene) and the short-term (Late-Pleistocene and Holocene) slip rates have been calculated for the TFS and TpFS using geomorphological and paleoseismological information, respectively. In the case of the TFS, the estimated minimum geomorphological slip rate ranges between 0.06 ± 0.02 mm yr^{-1} using the Pliocene age (5.34–2.58 Myr) of the Bañí-Solís domes (Ortuño et al., 2015) and a vertical displacement of 217 ± 10 m the topographic envelope of volcanic mesa reliefs is near profile B (Figs. 3A, 4A). The topographic throw should be considered a minimum, since the down-thrown block is filled with materials younger than the lava flows that at an undetermined depth.

A larger average slip rate is derived from the paleoseismological observations; in the Juanacatlan trenches, the accumulated displacement of unit *h* ranges between 1.39 ± 0.14 m (Juana 1E) and 1.85 ± 0.17 (Juana 1W). Because we have not an age for unit *h*, we have considered the age of unit *g* (12010-11620 BC modeled age, Table 2) as a good minimum estimate. With those values, we have obtained a slip rate of 0.12 ± 0.02 mm yr^{-1}. Other slip estimates can be obtained by considering younger units. For instance, unit *c*, which has a 11,710-10,780 BC modeled age (Table 2), is displaced vertically with a maximum throw of 0.72 ± 0.12 (Juana 2E) and 1.11 ± 0.25 (Juana1W). This gives a slip rate of 0.07 ± 0.03 mm yr^{-1}. The difference in slip rate, depending on the unit considered, appears to reflect the clustering of events affecting older units

The long-term minimum value of the maximum geomorphological slip rate for TpFS is obtained with a maximum observed throw across a single fault branch of 125 ± 10 m of lava flow surfaces from the Sierra Puruagua range complex (Fig. 4B, profile

A). This displacement value is minimum because the lava flow surfaces) in the downthrown block are covered by younger volcanic fall sequences. The age of these materials should be between 11.62 – 5.34 Myr and 2 Myr, based on Ar/Ar ages ages of the volcanic complex on the footwall of the Acambay fault and overlying pumice deposits (Norini et al., 2010; Pedrazzi et al., 2016). The resulting long-term slip rate (minimum value of a maximum slip rate) for the TpFS is 0.01 to 0.07 mm yr^{-1}. A short-term slip rate of 0.23 ± 0.03 mm yr^{-1} is estimated for the San Antonio fault, within the TpFS. This value is based on the 1.18 ± 0.1 m vertical displacement of unit *e* caused the fault inferred between trenches Tepux 1 and TEpux 2 and its corresponding age of 3515 - 3105 BC. The short-term slip rate value should be regarded as preliminary, because the existence of the buried fault could not be confirmed (suspected fault, **Fig. 8**).

To sum up, the long term and short-term slip rates along the western segment of the TFS might be very similar, and, have values ranging from 0.06 ± 0.02 (minimum long term) to 0.12 ± 0.02 mm yr^{-1} (maximum value of average short-term). For the TpFS, long-term slip rates are low, between 0.01 and 0.02 mm yr^{-1}, whereas the short-term estimated from the paleoseismological exposure is 0.23 ± 0.03 mm yr^{-1}. This last value is very uncertain, because it is inferred for a fault that could not be exposed.

The estimated slip rates in this study, both for the long term and short term, are within the lower range of the slip rate values reported for other faults in the Central TMVB. Published long-term slip rates for some of the Acambay Graben faults using the vertical displacement of markers older than 0.3 Myr vary between 0.02 and 0.18 mm yr^{-1} (Suter et al., 2001). Considering younger markers exposed in trenches, short-term slip rates obtained by other authors from paleoseismological data show a wide range of values, although larger slip values (compared to the long-term slip rates) are detected. Most slip rates inferred in paeloseismological studies are between 0.01 and 0.4 mm yr^{-1} (0.15 ± 0.02 mm yr^{-1} for the Acambay fault from Langridge et al., 2000; 0.23 - 0.37 mm yr^{-1} for the Pastores Western end from Ortuño et al., 2015; 0.22 - 0.24 mm yr^{-1} for the Venta de Bravo fault from Lacan et al., 2018; and 0.5 mm yr^{-1} for La Paloma fault from Israde, 1995, and Garduño-Monroy et al., 2009). Minor faults within the graben axis also show similar values to slip rates estimated in our study (e.g., 0.15 – 0.06 mm yr^{-1} for the San Mateo Fault from Sunyé-Puchol et al., 2015,). Lower values (0.03 mm yr^{-1}) provided by Langridge et al. (2013) for the Pastores fault could be related, in our opinion, to the fact that they only represent the slip of one fault branch in a geological section where the fault probably has more than one active branch.

7. Discussion

7.1 Primary vs secondary rupture and fault behavior within the TMVB

An imporant outcome of our study is that the central faults in the Acambay Graben can produce primary (seismogenic) ruptures. This is a new perspective as to date they had only historically behaved as secondary ruptures to major ruptures along the graben bounding faults. We have analyzed this double behavior by studying five different faults within the central Acambay Graben, exposed in eight natural outcrops and in three paleoseismological trenches.

Secondary behavior observed in the present study implies induced (triggered) small fault ruptures and is based on the variability of SEDs obtained at the Juanacatlan site, and in comparison, with historic ruptures (see below). Also, the observation of a cluster in the paleo-earthquake distribution suggests that the faults in the central TMVB are likely to show non-periodic behavior. However, full confirmation of their dual primary and secondary and their potential non-periodic behavior requires having a larger catalogue of paleoseismic observations.

7.1.1 Fault behavior of intra-graben Temascalcingo and Tepuxtepec faults

In this section, we explore the possible causes of the variation of the inter-seismic cycle (non-period behavior) and of SED (primary versus secondary behavior) observed in the Juanacatlan trenches. The earthquake chronology in Juanacatlan trenches suggests a non-uniform distribution of events through time with six events that occurred since 12,500-11,195 BC, of which three events (3, 4 and 5) occurred within a maximum of 1720 yrs span. An aperiodic behavior has also been observed in other faults within the Acambay Graben (Langridge et al., 2000, 2013, Ortuño et al., 2015, Sunyé-Puchol et al., 2015, Lacan et al., 2018).

The slip history shows variable SEDs, with values averaged in 0.46 ± 0.06 cm, representing a coefficient of variation (CoV) of 0.52 ± 0.03. This notable variability in SED is also found in other paleoseismic studies in the central TMVB (Table 4).

Variable primary rupture related to complex stress loading

The variability of SEDs and inter-seismic periods in the studied fault sections, could be a consequence of, at least, two processes: **1**) the fault complexity and the close spacing between the faults within the TMVB (up to 10 faults in some profiles perpendicular to the graben, Fig. 1) can led to fault interactions through stress loading; and **2**) similarly, the nearby volcanic centers can interact with the faults.

In complex faults systems, faults can be brought to failure, or away from it, through crustal stress changes caused by rupture of the neighboring faults (e.g., Stein, 1999). One of the consequences of this interaction is the clustering of earthquakes in time. In the geological record, clusters of earthquakes have been classically related to fault interaction and stress transfer in complex systems (e.g., Harris, 1998). Berryman et al., (2012) proposed that the degree of complexity of fault systems scales with the variability of the recurrence time. Accordingly, the periodicity of earthquakes varies between two end members: isolated and large (relatively fast) faults, such as the Alpine fault in New Zealand, tend to show a quasi-regular recurrence, while slower and networked systems are more prone to show clustered behavior The latter end member is exemplified by the normal faults of the Taupo Rift (New Zealand), where evidence from more than 50 paleoseismic trenches excavated across a complex network of branching-out and merging-in active faults, with narrow spacing (few hundreds of meters to 5 km across strike), suggest a high level of fault interaction (Nicol et al., 2006; 2009; Villamor et al., 2007). This interaction is not only reflected in highly variable interseismic time, but also in highly variable SEDs (the high level of fault connectivity produces faults ruptures with different magnitudes for a single fault). The large variability in SED and recurrence interval in the Taupo Rift causes also high variability in fault slip rate (Nicol et al., 2009).

We propose that the intra-arc extensional system represented by the TMBV is likely to be close to the aperiodic end-member, similar to the Taupo Rift. An aperiodic end-member is described as a system where horizontal extension is distributed along a large number of faults (5 to 10 according to Ego and Ansan, 2002), and where relatively slow structures show a non-periodic behavior.

An additional cause of variable recurrence could be the influence of volcanic crustal stress changes associated with volcanic unrest or eruption. As suggested for other volcanic areas (e.g., Walter et al., 2007; Villamor et al., 2011), the activity of faults near volcanic centers can trigger volcanic activity but also is influenced by it. Magma inflation and deflation, and dike intrusion can produce changes in crustal stress that can bring faults closer or away from failure (e.g., Villamor et al., 2011, and references therein). In this case, despite the final triggering mechanism by volcanic activity, fault ruptures are tectonic. In volcanic areas, where extension is mainly achieved by magmatism (by dike intrusion rather that tectonic faulting), surface faulting may be a consequence of shallow dike intrusion associated with small magnitudes (< M_w 5; e.g., 2005 Dabbahu rifting episode, Afar; Rowland et al., 2007). In this case surface faulting can be regarded as non-tectonic and thus is not associated with large magnitudes (M>6) (Villamor et al., 2011).

The comparison of faulting styles and rifting evolutionary stages for various rifts worldwide by Villamor et al. (2017) suggests that the TMBV has similarities with the southern sector of the Taupo Rift. There, important characteristics are the small volumes of volcanisms/magmatism and that extension is accommodated mainly by tectonic faulting (with a small percentage of dike intrusion; Gomez-Vascocelos et al., 2017). In such environments, surface faulting is mainly tectonic (although it can be primed by dike intrusion on occasions). Volcanic activity involving large volumes of material in the magma chamber is not reported for the Acambay Graben during the Late Pleistocene-Holocene in the study region. The only the occurrence of relative large volumes of volcanism area localized ignimbrites, possibly triggered by tectonic events (Aguirre et al., 2015; Ortuño et al., 2015; Lacan et al., 2018, this issue) in the last few thousands of years. While the comparison mentioned above suggests that the active fault displacements measured in our study are likely to be mainly tectonic, the acquisition of further and completer faulting and volcanism datasets within the Acambay Graben are needed to better understand if some surface fault displacements are non-tectonic.

Alternating primary and secondary faulting

We consider that the larger SEDs observed in the TFS and TpFS (between 60 and 100 cm) represent primary fault behavior. Their location at a distance >15 km to the major faults bounding the graben (Acambay and Venta de Bravo-Pastores faults, Fig. 1) leads to the inference that SEDs associated with secondary faulting on the TFS and TpFS should be similar or smaller to the secondary displacements during the Acambay earthquake of 1912 (i.e, <30 cm Fig.1). The 1912 earthquake caused coseismic cracks and minor slip in three faults located inside the graben, the Pastores, Temascalcingo and possibly San Mateo fault, located between 6 to 14 km from the main fault rupture. The re-interpretation of the original data reported by Urbina and Camacho (1913) led to the consideration that the secondary vertical displacements observed on those faults may have reached 30 cm (Suter et al., 1995; Langridge et al., 2000; Rodríguez-Pascua et al., 2012). SEDs in the Acambay Graben boundary faults from paleoseismological studies (Table 4) do not exceed 1 m. Thus, the maximum SEDs observed in this study are likely the result of primary ruptures along the Temascalcingo and San Antonio faults.

Together with the 1912 Acambay earthquake, the Edgecumbe earthquake (M_L 6.3; March 2nd, 1987) in the Taupo Rift (New Zealand) is a good example of extensive secondary faulting caused by a large earthquake in a volcanic extensional system.

During this earthquake, secondary faulting occurred along faults as far as 8 km away from the primary source (Edgecumbe fault) and exhibited a swarm-like distribution of secondary ruptures (Beanland et al., 1989). These secondary faults presented a wide variety of surface rupture lengths (from m to km) and vertical slips (from 0.8 to 0.035 m), which locally included subsidence deformation and post-seismic relaxation. Surface displacement combined with geodetic data allowed those authors to conclude that faulting on the primary source accounted for about three quarters of the total surface slip, whereas the rest of the slip was distributed among the secondary ruptures.

7.1.2 Maximum expected magnitude of primary ruptures

The fault scaling relationship proposed by Wesnousky (2008) is considered the most suitable for volcanic environments with thick (> 10 km) brittle crust (Stirling et al., 2013), as is the case of the TMVB. This relationship is based on fault surface length. We prefer not to use SED to calculate M_w because the SEDs are observed at a single location along the fault and thus they do not fully represent the average value required to appropriately derive the magnitude. Wesnousky (2008) equation is as follows:

$$M_w = 6.12 + 0.47 \log L$$

$$\sigma = 0.27 \text{ (in } M_w\text{)}$$

Considering that the total surface trace length of the faults corresponds to the maximum surface rupture length (L), we obtain a M_w 6.7 for the Temascalcingo fault (L=19 km) and a M_w 6.5 for the two segments of the San Antonio faults (L= 7.3 and 7 km). The possible combined rupture along the Temascalcingo and San Rafael faults (will produce a M_w 6.8 earthquake (L=35 km). This combined rupture is possible as the faults are aligned and both dip to the north. Also, the paleo-earthquake chronologies show matching intervals that are compatible with that scenario. The separation between the Temascalcingo and San Rafael faults (~5 km) might not represent a strength barrier, allowing the fault propagation. Such a rupture could have triggered movement at the San Antonio fault, which is antithetic to San Rafael fault. Any of the primary fault rupture scenarios mentioned above with M_w from 6.5 to 6.8 will produce strong ground shaking in the townships of the area, as Acambaro (near 60,000 inhabitans) Maravatío (more than 80,000 inhabitants). This proves the relevance of incorporating the TFS and TpFS as fault sources in seismic hazard estimates for the region.

8. Concluding remarks

The Temascalcingo and Tepuxtepec fault systems show morphological, structural and sedimentary features confirming their normal fault activity since the Late Miocene. Based on their geomorphological expression, they could be part of a single system within the Acambay Graben axis. The system consists of up to 20 normal fault segments arranged in a complex surface pattern with left steps and horse-splay terminations.

Eight natural outcrops and five paleoseismic trenches were analyzed to better understand fault kinematics and earthquake parameters. A dominant dip slip with minor left lateral component (only in traces with NW or NE trends) characterizes the slip motion of most of the faults investigated. The westernmost segment of the

Temascalcingo fault was studied at the Juanacatlan site, where a sequence of six surface ruptures was identified. These ruptures occurred after 12,500-11,195 BC and showed a clustered temporal distribution, with three events dated between 11,057 and 11,939 BC. In the Tepuxtepec system, the San Antonio trenches did not expose the main fault trace. Secondary faulting indicates that at least two rupturing events occurred in the area since 3105-3515 BC.

The variability in single event displacement (SEDs) observed at the Juanacatlan site suggests that the fault does not have a characteristic behavior, and that it probably ruptures as both primary and secondary in different events. Relatively large SEDs (up to 77 cm) suggest that the fault can produce primary ruptures. The length of the traces base on morphological expression the feasibility of simultaneous ruptures within the Temascalcingo and Tepuxtepec systems suggest that these faults can produce up to 6.8 M_w earthquakes. Secondary displacements on these faults could be triggered by distant primary ruptures on other faults within the Acambay Graben, as it happened during the 1912 Acambay earthquake, as well as by large volcanic eruptions.

The results presented here are only preliminary as there are still many large uncertainties. Within the central TMBV, more paleoseismic and Holocene volcanism studies are needed to clarify key issues such as the temporal and spatial slip-rate variability, and the distinction between tectonic and volcanic-triggered faulting, which has important implications in seismic hazard estimates. Nonetheless, the results presented here suggest scenarios in which strong ground will affect the central Mexico where the population has grown substantially in the last few decades. Our results can be utilized to create fault source models for future seismic hazard assessment in the region.

Acknowledgements

This study was supported by the Universidad Nacional Autonoma de Mexico (PAPIIT grants IA101615, IA102317, IN-104615 and IN112110) and by Consejo Nacional de Ciencia y Tecnología (CONACyT, Mexico) grant CB-2009-01-129010. Petra Štěpančíková was supported by the Czech Science Foundation Project Number 205/08/P521 and P210/12/0573, and the long-term conceptual development research organization RVO: 67985891. Pilar Villamor was support by New Zealand Ministry of Business, Innovation and Employment (Strategic Science Investment Fund). We are grateful to Tom Rockwell for revision of an earlier version of this manuscript. We are in debt with Ernesto López, Arturo López, Rosanna Bonasia, Lina Serrano, Hugo Dubé-Loubert, Danielle Dell'Erba, Maria Helbig, Gianluca Norini and Ivan Sunyé-Puchol for field assistance and scientific discussions. Thanks to the owners of the paleoseismological sites, who allowed us to excavate trenches and helped with logistics.

Supplementary Material

A.1. Photomosaics and general pictures of the trenches at Juanacatlan site.

A.2. Photomosaic and general pictures of the trenches at San Antonio site.

A.3. Geological map of the study area.

A.4. Sedimentary description of units exposed in the trenches and their interpretations.

A.5 Sketch with measurements of throws in Juanacatlan trenches.

A.6 Excel file with the calculation of throws and uncertainties in Juanacatlan trenches

A.7. Oxcal model for Juanacatlan site.

A.8. Shaded relief map with the drainage configuration of the Tepuxtepec system and the geomorphological map of the area published in Ramírez-Herrera, 1994.

References

References

Aguirre-Díaz, G.J., 1996. Volcanic stratigraphy of the Amealco caldera and vicinity, Central Mexican Volcanic Belt. Revista Mexicana de Ciencias Geológicas 13 (1), 10–51.

Aguirre-Díaz, G.J., Urrutia-Fucugauchi, J., Soler-Arechalde, A.M., McDowell, F.W., 2000. Stratigraphy, K-Ar ages, and magnetostratigraphy of the Acambay graben, central Mexican Volcanic Belt. In: Delgado-Granados, H., Aguirre-Díaz, G., Stock, J. M. (Eds.), Cenozoic tectonics and volcanism of Mexico: Boulder, Colorado, Geological Society of America Special Paper 334, 167–178.

Aguirre-Díaz, G., Ortuño, M., Zúñiga, R., Lacan, P., Persaud, M., 2012. Late Pleistocene-Holocene explosive volcanism in the Acambay graben: A change to the status of this zone of central Mexico to one of potential volcanic danger. Cities on Volcanoes 7, International Association of Volcanology and Chemistry of the Earth's interior, Colima, Mexico, Conference proceedings.

Aguirre, G., Pedrazzi, D., Lacan, P., Roldan-Quintana, J. Ortuño, M., Zúñiga, R., Audin, L., 2015. Quaternary volcanism in the Acambay graben, Mexican Volcanic Belt: Re-evaluation for potential volcanic danger in central Mexico. *AGU* Fall Meeting. American Geophysical Union, San Francisco, USA, *94*(49), Abstract V31B-3029.

Astiz-Delgado, L.M., 1980. Sismicidad en Acambay, Estado de México-el temblor del 22 de febrero de 1979. Ph.D. Thesis, Facultad de Ingeniería, Universidad Nacional Autónoma de México, Mexico.

Beanland, S., Berryman, K.R., Blick, G.H., 1989. Geological investigations of the 1987 Edgecumbe earthquake, New Zealand. New Zealand Journal of Geology and Geophysics 32 (1), 73–91. DOI: 10.1080/00288306.1989.10421390

Berryman, K., Cochran, U.A., Clark, K.J., Biasi, G.P., Langridge, R.M., Villamor, P., 2012. Major earthquakes occur regularly on an isolated plate boundary fault. Science 336 (6089), 1690–1693. DOI: 10.1126/science.1218959

Bronk Ramsey, C., 1995. Radiocarbon calibration and analysis of stratigraphy. The OxCal program. Radiocarbon 37 (2), 425–430.

Bronk Ramsey, C., 2001. Development of the radiocarbon program OxCal. Radiocarbon 43 (2A), 355–363.

Bronk Ramsey, C., 2008. Deposition models for chronological records. Quaternary Science Reviews 27 (1-2), 42–60. DOI:10.1016/j.quascirev.2007.01.019

Corominas, O., 2011. Estudio paleosismológico del sistema de fallas de Tepuxtepec, graben de Acambay, México. M.Sc. thesis, Universidad de Barcelona, Spain.

Dawers, N.H., Anders, M.H., 1995. Displacement-length scaling and fault linkage, Journal of Structural Geology, 17, 607-614.

De la Fuente, G.J., Verma, S.P., 1993. Catálogo de aparatos volcánicos de la parte centro-occidental del Cinturón Volcánico Mexicano. Geofísica Internacional 32 (2), 351-386.

Ego, F., Ansan, V., 2002. Why is the Central Trans-Mexican Volcanic Belt (102° 99°W) in transtensive deformation? Tectonophysics 359 (1-2), 189–208. DOI:10.1016/S0040-1951(02)00666-2

Ferrari, L., Orozco-Esquivel, T., Manea, V., Manea, M., 2012. The dynamic history of the Trans-Mexican Volcanic Belt and the Mexico subduction zone. Tectonophysics 522–523, 122–149. DOI:10.1016/j.tecto.2011.09.018

Fletcher, J., Teran, O.J., Rockwell, T.K., Oskin, M.E., Hudnut, K.W., Mueller, K., Spelz Madero, R.M., Akciz, S., Masana, E., Faneros, G., Fielding, E., Leprince, S., Morelan, A.E., Stock, J., Lynch, D.K., Elliot, A.J., Gold, P.O., Liu Zeng, J., González Ortega, J.A., Hinojosa Corona, A., González García, J.J., 2014. Assembly of a large earthquake from a complex fault system: Surface rupture kinematics of the 4 April 2010

El Mayor–Cucapah (Mexico) M_w 7.2 earthquake. Geosphere 10 (4), 797–827. DOI: https://doi.org/10.1130/GES00933.1

Garduño-Monroy, V.H., Pérez-Lopez, R., Israde-Alcantara, I., Rodríguez-Pascua, M.A., Szynkaruk, E., Hernandez-Madrigal, V.M., Garcia-Zepeda, M.L., Corona-Chavez, P., Ostroumov, M., Medina-Veja, V.H., Garcia-Estrada, G., Carranza, O., Lopez-Granados, E., Mora-Chaparros, J.C., 2009. Paleoseismology of the southwestern Morelia-Acambay fault system, central Mexico. Geofísica Internacional 48 (3), 319–335.

Harris, R.A., 1998. Introduction to special section: stress triggers, stress shadows, and implications for seismic hazard. Journal of Geophysical Research 103 (B10), 347–358. DOI: 10.1029/98JB01576

Israde, I., 1995. Bacini lacustri del settore centrale dell’Arco Vulcanico Messsicano: Stratigrafia ed evolu-zione sedimentaria basata sulle diatomee. Ph.D. Thesis, Universita degli Studi di Milano, Italia.

Johnson, C.A., Harrison, C.G.A., 1989. Tectonics and volcanism in central Mexico: A Lansat Thematic Mapper perspective. Remote Sensing of Environment 28, 273–286.

Johnson, C.A., Harrison, C.G.A., 1990. Neotectonics in central Mexico. Physics of the Earth and Planetary Interiors 64 (2-4), 187-210. DOI: 10.1016/0031-9201(90)90037-X

Lacan, P., Zúñiga, R., Ortuño, M., Persaud, M., Aguirre, G., Langridge, R., Villamor, P., Perea, H., Štěpančíková, P., Carreon, D., Cerca, M., Suñe Puchol, I., Corominas, O., Audin, L., Baize, S., Lawton, T., Rendón, A., 2013. Paleoseismological History of the Acambay Graben (Central Mexico). *AGU* Fall Meeting. American Geophysical Union, San Francisco, USA, *94*(49), Abstract T23C-2591.

Lacan, P., Ortuño, M., Audin, L., Perea, H., Baize, B., Aguirre-Díaz, G.J., Zúñiga, R., 2018. Sedimentary evidence of historical and prehistorical earthquakes along the Venta de Bravo Fault System, Acambay Graben (Central Mexico). Sedimentary Geology, DOI: https://doi.org/10.1016/j.sedgeo.2017.12.008

Langridge, R., Weldon, R., Moya, J., Suárez, G., 2000. Paleoseismology of the 1912 Acambay earthquake and the Acambay-Tixmadejé fault, Trans-Mexican Volcanic Belt. Journal of Geophysical Research 105 (B2), 3019–3037. DOI: 10.1029/1999JB900239

Langridge, R.M., Persaud, M., Zúñiga, F.R., Aguirre-Díaz, G.J., Villamor, P., Lacan, P., 2013. Preliminary paleoseismic results from the Pastores fault and its role in the seismic hazard of the Acambay graben, Trans-Mexican Volcanic Belt, Mexico. Revista Mexicana de Ciencias Geológicas 30 (3), 463-481.

Lienkaemper, J.J., Bronk Ramsey, C., 2009. OxCal: Versatile tool for developing paleoearthquake chronologies-A primer. Seismological Research Letters 80 (3), 431-434. DOI: 10.1785/gssrl.80.3.431

Martínez Reyes, J., Nieto-Samaniego, A.F., 1990. Efectos geológicos de la tectónica reciente en la parte central de México. Revista del Instituto de Geología de la Universidad Nacional Autónoma de México 9, 33–50.

McCalpin, J.P., 2009. Paleoseismology (second edition). Academic Press-Elsevier, Amsterdam.

Mooser, F., 1972. The Mexican Volcanic Belt-Structure and tectonics. Geofísica Internacional 12, 55-70.

Nicol, A., Walsh, J.J., Berryman, K., Villamor, P., 2006. Interdependence of fault displacement rates and paleoearthquakes in an active rift. Geology 34 (10), 865–868. DOI: https://doi.org/10.1130/G22335.1

Nicol, A., Walsh, J., Mouslopoulou, V., Villamor, P., 2009. Earthquake histories and Holocene acceleration of fault displacement rates. Geology 37 (10), 911–914. DOI: https://doi.org/10.1130/G25765A.1

Norini, G., Groppelli, G., Lagmay, A.M.F., Capra, L., 2006. Recent left-oblique slip faulting in the central eastern Trans-Mexican Volcanic Belt: Seismic hazard and geodynamic implications. Tectonics 25 (4), TC4012. doi: 10.1029/2005TC001877

Norini, G., Capra, L., Borselli, L., Zúñiga, F.R., Solari, L., Sarocchi, D., 2010. Large scale landslides triggered by Quaternary tectonics in the Acambay graben, Mexico. Earth Surface Processes and Landforms 35 (12), 1445-1455. **DOI:** 10.1002/esp.1987

Ortuño, M., Zúñiga, R., Corominas, O., Perea, H., Ramírez-Herrera, M.T., Štepancíková, T., Villamor, P., Aguirre-Díaz, G.J., Norini, G., 2011. Caracterización de fallas sismogenéticas en el centro del Cinturón Volcánico Trans–Mexicano: Resultados Preliminares. XIV Latinoamerican Conference of Geology, Medellín, Colombia, Abstracts 165–166.

Ortuño, M., Zúñiga, R., Corominas, A., Perea, H., Ramírez-Herrera, M.T., Štepancíková, P., Villamor, P., Norini, G., 2012. Paleoseismology of the Venta de Bravo, Tepuxtepec and Temascalcingo faults (Transmexican Volcanic Belt). Reunión anual 2012 de la Unión Geofísica Mexicana, Puerto Vallarta, Mexico, abstract SE11-8.

Ortuño, M., Zúñiga, F.R., Aguirre-Díaz, G.J., Carreón-Freyre, D., Cerca, M., Roverato, M., 2015. Holocene paleo-earthquakes recorded at the transfer zone of two major faults: the Pastores and Venta de Bravo faults (Trans-Mexican Volcanic Belt). Geosphere 11 (1), 160-184. DOI: https://doi.org/10.1130/GES01071.1

Pedrazzi, D., Aguirre Díaz, G., Sunyé-Puchol, I., Bartolini, S., Geyer, A., 2016. Volcanic activity in the Acambay Graben: a < 25 Ka subplinian eruption from the Temascalcingo volcano and implications for volcanic hazard. General Assembly 2016. European Geosciences Union, Vienna, Austria, Abstract 6552.

Ramírez-Herrera, M. T. 1994. Tectonic geomorphology of the Acambay graben, Mexican Volcanic Belt, PhD thesis, University of Edinburgh, 251 pp

Ramírez-Herrera, M.T., 1996. Morphological evidence for neotectonic activity and seismic hazard in the Acambay graben, Mexican Volcanic Belt. In: Slaymaker, O. (ed.) John Wiley & Sons Ltd, Geomorphic hazards, 29-41.

Ramírez-Herrera, M.T., 1998. Geomorphic assessment of active tectonics in the Acambay graben, Mexican volcanic belt. Earth Surface Processes and Landforms 23, 317–332.

Ramírez-Herrera, M.T., Summerfield, M.A., Ortiz-Pérez, M.A., 1994. Tectonic geomorphology of the Acambay graben, Mexican Volcanic Belt. Zeitschrift für Geomorphologie 38, 151–168.

Reimer, P.J., Bard, E., Bayliss, A., Beck, J.W., Blackwell, P.G., Ramsey, C.B., Buck, C.E., Cheng, H., Edwards, R.L., Friedrich, M., Grootes, P.M., Guilderson, T.P., Haflidason, H., Hajdas, I., Hatte, C., Heaton, T.J., Hoffmann, D.L., Hogg, A.G., Hughen, K.A., Kaiser, K.F., Kromer, B., Manning, S.W., Niu, M., Reimer, R.W., Richards, D.A., Scott, E.M., Southon, J.R., Staff, R.A., Turney, C.S.M., Van der Plicht, J., 2013. Intcal13 and Marine13 Radiocarbon Age Calibration Curves 0-50,000 Years Cal BP. Radiocarbon 55 (4), 1869-1887. DOI: https://doi.org/10.2458/azu_js_rc.55.16947

Roberts, G. P., Cowie, P., Papanikoloau, I., Michetti. A. M., 2004. Fault scaling relationships, deformation rates and seismic hazards: an example from Lazio-Abruzzo region, central Italy. Journal of Structural Geology, 26, 377-398.

Rodríguez-Pascua, M.A., Garduño-Monroy, V.H., Pérez-López, R., Perucha-Atienza, M.A., Isdrade-Alcántara, I., 2012. The Acambay earthquake of 1912, revisited 100 years after. 3rd INQUA-IGCP-567 International Workshop on Active Tectonics, Paleoseismology and Archaeoseismology, Morelia, México, pp. 167–160.

Rodríguez-Pérez, Q., Zúñiga, F.R., Lacan, P., 2017. Paleoseismological uncertainty estimation in the Acambay region, Central Mexico. Geofísica Internacional 56 (3), 255-268.

Roldan-Quintana, J., Aguirre-Díaz, G., Rodríguez-Castañeda J.L., 2011. Depósito de avalancha de escombros del volcán Temascalcingo en el graben de Acambay, Estado de México. Revista Mexicana de Ciencias Geológicas 28 (1), 118-131.

Rowland, J.V., Baker, E., Ebinger, C.J., Keir, D., Kidane, T., Biggs, J., Hayward, N., Wright, T.J., 2007. Fault growth at a nascent slow-spreading ridge: 2005 Dabbahu rifting episode, Afar. Geophysical Journal International 171 (3), 1226-1246. DOI: 10.1111/j.1365-246X.2007.03584.x

Sánchez-Rubio, G., 1984. Cenozoic volcanism in the Toluca-Amealco region, central Mexico. Ph.D. thesis, Imperial College of Science and Technology, University of London, United Kingdom.

Stein, R. S., 1999. The role of stress transfer in earthquake occurrence. Nature, 402, 605- 609.

Stirling, M., Rhoades, D., Berryman, K., 2002. Comparison of earthquake scaling relations derived from data of the instrumental and preinstrumental era. Bulletin of the Seismological Society of America 92 (2), 812–830. DOI: https://doi.org/10.1785/0120000221

Stirling, M., Goded, T., Berryman, K., Litchfield, N., 2013. Selection of earthquake scaling relationships for seismic-hazard analysis. Bulletin of the Seismological Society of America 103 (6), 2993–3011. DOI : 10.1785/0120130052

Sunyé-Puchol, I., Lacan, P., Ortuño, M., Villamor, P., Audin, L., Zúñiga, F.R., Langridge, R.M., Aguirre-Díaz, G.J., Lawton, T.F., 2015. La falla San Mateo: Nuevas evidencias paleosismológicas de fallamiento activo en el graben de Acambay, México. Revista Mexicana de Ciencias Geológicas 32 (3), 361-375.

Suter, M., 2014. Comment on “Estimation of ground motion in Mexico City from a repeat of the M ~ 7:0 Acambay earthquake of 1912” by Shri Krishna Singh, Arturo Iglesias, Mario Ordaz, Xyoli Pérez-Campos, and Luis Quintanar. Geological Society of America Bulletin 104 (5), 2562-2564. DOI: https://doi.org/10.1785/0120140126

Suter, M., 2016. Structure and Holocene rupture of the Morelia Fault, Trans-Mexican Volcanic Belt, and their significance for seismic hazard assessment. Bulletin of the Seismological Society of America 106 (5), 2376-2388. DOI: https://doi.org/10.1785/0120160092

Suter, M., Quintero, O., Johnson, C.A., 1992. Active faults and state of stress in the central part of the Trans-Mexican Volcanic Belt, Mexico. The Venta de Bravo fault. Journal of Geophysical Research 97 (B8), 11983–11993. DOI: 10.1029/91JB00428

Suter, M., Quintero, O., López, M., Aguirre-Díaz, G.J., Ferrar, E., 1995. The Acambay graben: Active intraarc extension in the Trans-Mexican Volcanic Belt. Tectonics 14 (6), 1245–1262. DOI: 10.1029/95TC01930

Suter, M., Carrillo-Martínez, M., Quintero-Legorreta, O., 1996. Macroseismic study of earthquakes in the central and eastern parts of the Trans-Mexican Volcanic Belt. Bulletin of the Seismological Society of America 86 (6), 1952–1963.

Suter, M., López-Martínez, M., Quintero-Legorreta, O., Carrillo-Martínez, M., 2001. Quaternary intra-arc extension in the central Trans-Mexican volcanic belt. Geological Society of America Bulletin 113 (6), 693–703. DOI: https://doi.org/10.1130/0016-7606(2001)113<0693:QIAEIT>2.0.CO;2

Urbina, F., Camacho, H., 1913. La zona megaseísmica Acambay-Tixmadejé, Estado de México, conmovida el 19 de noviembre de 1912. Boletín del Instituto Geológico de México 32, 1-125.

Velázquez-Bucio, M.M., Garduño-Monroy, V.H., Soria-Caballero, D.C., Israde-Alcántara, I., Rodríguez-Pascua, M.A., Pérez-López, R., 2012. Coseismic stratigraphy in holocene lacustrian sequences of San Pedro el Alto, estado de México. 3rd INQUA-IGPC-567, International Workshop on Active Tectonics, Paleoseismology and Archaeoseismology, Morelia, Mexico, pp. 195-198.

Villamor, P., Van Dissen, R., Alloway, B.V., Palmer, A.S., Litchfield, N., 2007. The Rangipo fault, Taupo rift, New Zealand: An example of temporal slip rate and single-event displacement variability in a volcanic environment. Geological Society of America Bulletin 119 (5-6), 529–547. DOI: https://doi.org/10.1130/B26000.1

Villamor, P., Berryman, K.R., Nairn, I.A., Wilson, K., Litchfield, N., Ries, W., 2011. Associations between volcanic eruptions from Okataina volcanic center and surface rupture of nearby active faults, Taupo rift, New Zealand: Insights into the nature of volcano-tectonic interactions. Geological Society of America Bulletin 123 (7-8), 1383–1405. DOI: https://doi.org/10.1130/B30184.1

Villamor, P., Berryman, K.R., Ellis, S.M., Schreurs, G., Wallace, L.M., Leonard, G.S., Langridge, R.M., Ries, W.F., 2017. Rapid evolution of subduction-related continental intraarc rifts: The Taupo Rift, New Zealand. Tectonics 36 (10), 2250–2272. DOI: 10.1002/2017TC004715

Walter, T.R., Wang, R., Zimmer, M., Grosser, H., Lühr, B., Ratdomopurbo, A., 2007. Volcanic activity influenced by tectonic earthquakes: static and dynamic stress triggering at Mt. Merapi. Geophysical Research Letters 34 (5), L05304. DOI: 10.1029/2006gl028710.

Wells, S. G., Bullard, T. F., Menges, C. M., Drake, P. G., Karas, P. A., Kelson, K. I., Ritter, J. B. and Wesling, J. R., 1988. Regional variations in tectonic geomorphology along a segmented convergent plate boundary, Pacific coast of Costa Rica. Geomorphology, 1, 239–265

Wesnousky, S.G., 2008. Displacement and geometrical characteristics of earthquake surface ruptures: Issues and implications for seismic hazard analysis and the process of earthquake rupture. Bulletin of the Seismological Society of America 98 (4), 1609–1632. DOI: 10.1785/0120070111

Zúñiga, F.R., Suárez, G., Figueroa-Soto, A., Mendoza, A., 2017. A first order seismotectonic regionalization of Mexico for seismic hazard and risk estimation. Journal of Seismology 21, 1295-1322. DOI: 10.1007/s10950-017-9666-0

Table Captions

Table 1. Summary of information from structural outcrops along the Temascalcingo and Tepuxtepec fault systems. Location of outcrops is included in Fig. 3. Photographs, stereoplots and sketches of some of the sites are shown in Fig. 5a and b.

Table 2. Dating results. Laboratories providing results are Arizona University Radiocarbon Laboratory and Beta Analytic Inc, Miami headquarters; Most results are AMS., except those marked with (1) which refer to conventional dating. The calibrated

ages have been obtained using OxCal 4.2 software (Bronk Ramsey, 2008), 2σ uncertainty and the IntCal13 curves (Reimer et al., 2013). All ages are rounded to the nearest multiple of 5. Calibrated ages obtained through an OxCal stratigraphic sequence model are indicated with a (*) symbol.

Table 3. Summary of evidence for surface rupture identified in Juana 1 and 2 trench walls . Vertical offset measured for each fault is given. The difference in CT (cumulated throw) between consecutive events is used to calculate the single event displacement (SED).

Table 4. Surface rupture length (SRL) and single event displacement (SED) observed at different faults within the TMVB from paleoseismological studies.

Figure Captions

Figure 1. Main faults within eastern Acambay-Morelia fault system and instrumental seismicity (1956 – 2016). Main active faults have been mapped using 30 m resolution digital topography and aerial photographs. The studied fault systems are framed by the white rectangles. Structural outcrops (kinematic stations) are indicated with numbered yellow triangles. Information on the two largest earthquakes occurred in the area since the beginning of the 20^{th} century is included: the red star is the epicenter of the 1912 Acambay earthquake (Ms = 6.7, according to Suter et al., 1995); and the light blue star shows the location and focal mechanism of the Maravatio earthquake (1979, body wave magnitude, mb = 5.3) provided by Astiz-Delgado (1980). PNF, Paquisihuato north fault. PSF, Paquisihuato south fault. Inset: Location of the study area within the intra-plate

tectonic setting of Mexico. Faults referred in text are: 1, Acambay graben system; 2, Tenango fault; 3, faults near Morelia city (Morelia, Tarímbaro and La Paloma faults). Main faults have been drawn with thicker lines. Modified from Lacan et al. (2013).

Figure 2a. Field photos showing the geomorphological expression and Quaternary activity of the Temascalcingo fault. Location of photo viewpoints in Figures 1 and 3A. A: segment TF1; B and C: segment TF2.

Figure 2b. Field photos showing the geomorphological expression of Quaternary activity of the Tepuxtepec fault systems. Location of photo viewpoints in Figures 1 and 3B. D: San Rafael fault; E: Taranda fault; F: Paquishihuato North fault, separating lavas (to the south) from pyroclastic fall deposits (to the north).

Figure 3. Geomorphologic map of the studied faults and location of the outcrops mentioned in text. A: Temascalcingo fault system. B: Tepuxtepec fault system. Main faults have been drawn with thicker lines. Some of the photo viewpoints in Figure 2 are indicated with an eye symbol.

Figure 4. Topographic profiles analyzed for the Temascalcingo (A) and Tepuxtepec (B) faults: perpendicular profiles with vertical exaggeration x 2.5 (upper part); and parallel profiles with vertical exaggeration x 10 (lower part). In the parallel profiles, a solid line indicates the top of scarp and a discontinuous line, the base. Location of the cross sections in Figure 3.

Figure 5a. Photographs, sketches and structural data from analysis of exposures along the Temascalcingo fault. Location of kinematic stations in Figure 1 and detailed descriptions in Table 1. A: Outcrop of the Temascalcingo fault in a quarry in the Cerro Pelón (station 1); B: Outcrop of the Temascalcingo fault in quarry near La Huerta village (station 2); C: Outcrop of the Temascalcingo fault in quarry at the top of Temascalcingo volcano (station 3).

Figure 5b. Photographs, sketches and structural data of exposures along the Tepuxtepec, Paquishihauto San Antonio and San Rafael faults. Location of kinematic stations in Figure 1 and detailed descriptions in Table 1. D: exposure of one of the strands of the Tepuxtepec fault at a creek (station 4); E: Road cut exhibiting faulting of the present-day soil and alluvial and volcanic deposits of unknown age by the Paquishihauto fault (station 5); F: Outcrop of the San Antonio fault in a quarry next to San Antonio village (station 6); G: Outcrop of a San Antonio secondary fault at a creek (the fault has no geomorphic expression; station 7); H: natural outcrop of San Rafael fault (station 8).

Figure 6. Paleoseismological log of Juana 1 and 2 trenches at Juancatlan site, Temascalcingo fault.

Figure 7. Sequence restoration of the surface rupturing events inferred in Juana 1W trench, Temascalcingo fault. The sequence of events has been depicted in six steps (A-F) showing the geometry of layers after each event and after deposition of subsequent units.

Figure 8. Paleoseismological log of the Tepux 1, 2, and 3 trenches, Tepuxtepec fault.

Figure 9. Age constraints of paleoseismic events identified at different sites. The dating results marked in red are considered outliers and are not incorporated into the geochronological model.

Table 1

Temascalcingo system		
	Outcrop description	**Location**
Station 1 (Fig 5A)	E-W fault with dominant dip slip with a small right lateral component. Site at the step over of fault segments TscF2 and TscF3. The fault trace offset the surface. Faulting along a main fault oriented N080-090E/70N separates black and red scoria units and several secondary conjugate faults. Faults found in a small creep to the East show orientations of N110-115E/60-70ºN for the TscF2 across the volcanic mesa reliefs of the Bañi-Solís domes.	Quarry excavated in El Ruedo cinder cone: N19°55'58.08" W100°04'42.95" Creep outcrop N19°54'58.42" W100°02'18.15"
Station 2 (Fig. 5B)	ESE-WNW fault with dominant dip slip with a small left lateral component. Site at the middle of a slope formed by the cumulated activity of the TscF2. The faults exposed are secondary faults parallel to the morphological trace and oriented N096-118E/60N; with pitch 85ºW (F1) and a fault without morphological expression oriented N042-074E/85NW (F2), interpreted as an inactive conjugate fault of F1. Rocks affected by F1 are highly weathered dacitic breccias from the Bañí dome put next to a pyroclastic fall deposit deposit that mantles the slope. Fault F2 separates the dome from a fluvio-volcanic sequence containing, from top to bottom, coarse fluvial conglomerate, a blocky ignimbrite with a paleosoil developed on top and a block-and-ash flow deposit.	Quarry located near La Huerta village: N19°54'52.35" W100°01'52.92"
Station 3 (Fig. 5C)	ENE-WSW normal fault. Fault plane oriented N080-082E/60NW separating black and gray altered scoria units but not presenting geomorphic expression in the landscape. The fault affects a cinder cone located on the Eastern border of the Temascalcingo Caldera.	Quarry 3 km to the east of San Pedro village: N19°53'44.06" W99°56'28.93"
Tepuxtepec system		
	Outcrop description	**Location**
Station 4 (Fig. 5D)	Secondary fault separating lavas (to the north) from intraplinian pyroclastic surge deposits made of alternating pumice-fall out and ash units (to the south). The pyroclastic deposits are exposed by near 10 m incision of the river and are affected by a set of faults oriented N065E/70N, N70E/70N and N120E/80N showing sigmoidal structures.	Creek exposure near El Botín village: N19°59'20.75" W100°18'2.77"
Station 5 (Fig. 5E)	Secondary normal fault with ENE-SWS trend and north dip. It affects volcanic fall deposits, recent alluvial deposits and the present day soil. The volcanic sequence is made up of an alternation of lapilli and ash layers. In the downthrown, an artificial pond has been built bounding the fault scarp to the north. The fault zone is made of three fault branches exposed along the road cut of the dirty road heading north. The fault branch along the road cut is defined by three main fault branches (A, B and C,) which show fault zones 50-70 cm wide, with tectonic foliation and orientations varying from N065E/60N to 85N. Slickenlines in the main fault are oriented 57/332 indicating a main dip component of movement the main faults. Antithetic faults are oriented N70E/60S. With the exception of the main fault branches, that affect the soil top layer, other faults within the deposits are synsedimentary, since they not affect the upper layers of the volcanic deposit.	Road cut west of Estancia de Paquishihuato village: N19°56'55.74" W100°24'32.47"
Station 6 (Fig. 5F)	Compressive structure (positive flower) developed in a fault relief zone (oriented NNW-SSE) along the E-W normal San Antonio fault (south dip and minor left lateral component). It affects volcanic fall deposits with lapilli grain size and yellow-ochre. It is composed by angular clasts of felsic, well selected and with small fraction (5%) of lithic clasts. The volume and distribution of the deposit indicate a plinian eruption, probably coming from the Altamirano volcano (see Pedrazzi et al., 2016). We observed 9 fault planes. Among them, 5 fault planes (020/65, 060/85, 210/74, 202/72 and 220/86) separating the volcanic fall material from a gray silt containing reworked volcanic material, probably from fluvio-lacustrian origin. Other 4 fault planes (018/42, 132/89, 224/74, 228/85) are developed within the fall deposit and form part of the internal faults of the positive flower structure. The fault zone is characterized by a fault gouge and a fault mirror with slicken-	Quarry: N19º59'13.26" W100º13'51.73"

	lines oriented 51/135 and 70/172 in the plane 220/86.	
Station 7 (Fig. 5G)	Reverse fault with left lateral component. Fault with no surface expression, probably secondary faulted related to a transpression bend along San Antonio fault. The affected rocks are a sequence of ca 12 m thick of volcanic fall material (mainly felsic, of variable size felsic pumice to lapilli) and a colluvial deposit of dacitic centimetric blocks (cm in diameter). An upper alluvial deposit lies unconformably and seals the fault. It is interpreted as part of the alluvial infill of the San Antonio creek, parallel to the fault, preceding present-day incision. In this station we observe several families of fractures (047/75, 059/76, 066/89, 088/77, 230/88, 233/86, 240/85) developed within the lapilli layers. The main fracture zone contains a reddish clay material, probably corresponding to a fault gouge. In the fault plane oriented 047/75, slickenlines are oriented 49/337.	Creek exposure N 19º58'58.88'', W100º13'20.34''
Station 8 (Fig. 5H)	San Rafael normal fault with a north dip. Only the southern half of the Cerro Pelón cineritic cone is preserved, being the northern side downthrown and covered by most recent deposits. The erosion has exposed fault planes showing a sigmoidal structure and oriented N065E/54NW, N080E/68N and N088E/70N, affecting reworked volcanic and alluvial material.	Northern slope of the Cerro Pelón cone: N19º57'59.89'' W100º14'17.25''

Table 1. Summary of the structural outcrops studied along the Temascalcingo and Tepuxtepec fault systems. Location of the outcrops is included in Fig. 3; Photographs, stereoplots and sketches of some of the sites are shown in Fig. 5a and b.

Table 2

Sample name (unit)	Radiocarbon Age (years BP)	Calibrated Age (AD/BC)	Type of sample	Laboratory
Juanacatlan trenches				
JUA 2-7 (b)	4195 ± 95	3020 – 2495 BC*	Soil (bulk)	Arizona Univ .
JUA 2-5 (c’)	11710 + 395/-375	11710-10780 BC*	Soil (bulk)	Arizona Univ .
JUA 2-1 (d)	12721 ± 92	13525-12790 BC	Charcoal	Arizona Univ .(1)
JUA 2-6 (d)	15370 +320/-310	17445-15980 BC	Soil (bulk)	Arizona Univ .
JUA 1-1 (g)	11905 ± 65	12010-11620 BC*	Charcoal	Arizona Univ .(1)
JUA 1-FG-1 (g)	11845 +240/-230	12500-11195 BC	Soil (bulk)	Arizona Univ .
JUA 2-3 (h)	2830 ± 85	1220-815 BC	Soil (bulk)	Arizona Univ .
Tepuxtepec trenches				
TEPUX 3.7 (*b1*)	3941 ± 44	2570-2295 BC	Charcoal	Arizona Univ .(1)
TEPUX-2 (*e*)	4590 ± 40	3515 - 3105 BC	Charcoal	Beta Analytics.
T-2 16F (*d*)	11950 ± 160	12255-11495 BC	Soil (bulk)	Arizona Univ .

Table 2. Dating results. Laboratories providing results are Arizona University Radiocarbon Laboratory and Beta Analytic Inc, Miami headquarters; Most results are AMS., except those marked with (1) which refer to conventional dating. The calibrated ages have been obtained using OxCal 4.2 software (Bronk Ramsey, 2008), 2σ uncertainty and the IntCal13 curves (Reimer et al., 2013). All ages are rounded to the nearest multiple of 5. Calibrated ages obtained through an OxCal stratigraphic sequence model are indicated with a (*) symbol.

Table 3

Event (Bracket. units)	Juana 1E trench	Juana 1W trench	Juana 2E trench	Juana 2W trench	Comments
Ev. 1 a/b	*Fracture on F2 sealed* by unit *a* -*Displacement* (possible) on M CT 20 ± 4 cm (=SED)	CT 36 ± 7 cm probably inherited throw (=SED)	*Fractures on F2 sealed* by unit *a* - CT 15 ± 14 cm (= preferred SED)	-*Fractures on F4' sealed* by unit *a* -*Displacement of the base of b* on F5' (24 cm) MF (min. 18 – 38 cm); -*Fissures* infilled on F10' -CT 15 ± 0 cm (=SED)	Clearest evidence of surface rupture in J 2W.
Ev.2 b/c	-*Tilting* (~25º N) -*Displacement on* F4N (-3.5 cm) on MF (37 cm) *CT 80 ± 6 cm (60 ± 3 cm SED)*	- *Tilting* (~23º N) -*Displacement* on MF (39 cm) on F8' (-7.5 cm). *CT 110 ± 25 cm (75 ± 10 cm SED)*	- *Fracture* on F9 -*Fissured* with faulted material on F2, F6 and F8 *CT 72 ± 12 cm (57 ± 3 cm SED)*	- *Fractures* on F 12' and F8' -*Displacement* on MF (19 cm); F3'' F5' (25 cm); F8' (-22 cm), F11' (-17 cm). -*Tilting* (possible) along faults F4' to MF -*Fissures with faulted material* on F5' *CT 93 ± 31 cm (78 ± 17 cm SED)*	Clear fault generated scarp; Unit *c* not deposited or not preserved on up-thrown wall
Ev. 3 c/d	-*Fracture* on F10 sealed by unit c - *Displacement on* MF (> 13 cm, ~20 cm) *CT 93 ± 10 cm (12 ± 4 cm SED)*	-*Displacement* on MF (31 cm, considering surface not leveled); F5' (20 cm); F6' (17 cm); F7'' (8 cm). -*Faulted colluvial wedge* (by F6' , F7' and MF) *CT 136 ± 16 cm (25 ± 2 cm SED)*	-*Fractures F2 (open fracture)* -*Displacement on F5 (35 cm)* - SED calculated in next event	-*Displacement on* MF (15 cm) F4'N; F9' (-13 cm); - SED calculated in next event	Fault generated scarp suspected from geometry of unit c, which overlaps the scarp. Slip analyzed together with event 4 for J 1E, J 2E and J 2W
Ev.4 d/f	-*Fractures* sealed by unit d -*Displacement* on MF (38 cm); F4S (4 cm); F4S (3 cm). - CT 107± *8 cm (72 ± 9 cm SED)*	--*Displacement* on MF, min. *CT 137 ± 25 cm (79 ± 8 cm SED)*	No distinctive evidence-as unit F is not recorded in this trench Possibly, previous scarp mantled by unit d CT 102 ± *38 cm (SED =30 ± 15 cm)*	No distinctive evidence Possibly, previous scarp mantled by unit d CT 122 ± *21 cm (SED =29 ± 7 cm)*	Colluvial wedge on top of unit *f* (under unit *d*).
Ev. 5 F (d) /h (g)	-*Fractures* sealed by f'(f'') (F1 and F5-8, F11) -*Displacement* on F4 (4 cm) F5 (7 cm); on MF (min. 42 cm; min. thickness of *h*) - CT 139 ± 14 cm *(32 ± 5 cm SED)*	-*Fractures* sealed by f'(on both blocks). -*Displacement* on MF (min. 46 cm; min. thickness of *h*) - CT 185 ± 17 cm (48 ± 6 cm SED)	-*Fractures* sealed by *d* (F10, F4) -Counter-slope *tilting* of unit *h* -*Displacement* on MF (40 cm) apparently not affecting unit d - CT 172 ± 26 cm *(70 ± 7 cm SED)*	-*Displacement* on F2' (-11 cm) F3' *CT 56 ± 30 cm (34 ± 7 cm SED)*	Generation of space for deposition of re-worked ignimbrite (unit *h*) and channel infill (unit *g*) on the downthrown block.

Ev. 6 **h/i**		-*Fractures* sealed by unit *h* on F3, between F2 and MF *CT 228 ± 25 cm (57 ± 3 cm SED)*	-*Fractures* sealed by unit h. Not clear but perhaps some fractures between F2'-F3' and between F10' and F11' -*Displacement* of unit i, on MF (14 cm) *CT 226 ± 35 cm (70 ± 4 cm SED)*	Poorly constrained, possible multievent.

CT= cumulated throw; SED = single event displacement.

Table 3. Summary of the evidence of surface rupture identified in each of the trench walls of Juana 1 and 2. The vertical offset inferred from each fault is given. Offsets in some individual faults are locally exaggerated by opening and near surface vertical collapse. The difference in CT (cumulated throw) between consecutive events is used to calculate the single event displacement (SED).

Table 4

Fault name	Max. (min) SED	SRL (km)	Type of faulting	Reference
Acambay bounding faults				
Acambay	62/74 (46/58)	42	Primary, complex faulting during 1912 EQ	Langridge et al., 2000
Pastores	50 (<24)	50	Primary and co-seismic opening of fractures (debated)	Rodríguez-Pascua et al., 2012; Langridge et al. 2013
Pastores western end	37 (<29)	20.4	Transfer zone, perhaps only secondary	Ortuño et al., 2015
Venta de Bravo	100 (18)	47.7		Lacan et al, (2018)
Central Acambay graben faults (axis faults)				
San Mateo	150 (52)		Primary + secondary	Sunyé-Puchol et al., 2015
Temascalcingo	75 (22/39)	19 (three segments of 10.6, 7.3 and 6.1)	Primary + secondary	This study
San Antonio	80/100 (25)	Tepuxtepec: 8 (3.5 and 4.5) San Antonio: 7	Perhaps only secondary fault	This study
Morelia fault system				
La Paloma (West-Morelia fault segment)	40/50	12		Garduño-Monroy et al., 2009
Morelia fault	185 (46)	14		Suter, 2016

Table 5. Surface rupture length (SRL) and single event displacement (SED) observed at different faults within the TMVB through paleoseismological studies.

Figure 1 (Color)
Click here to download high resolution image

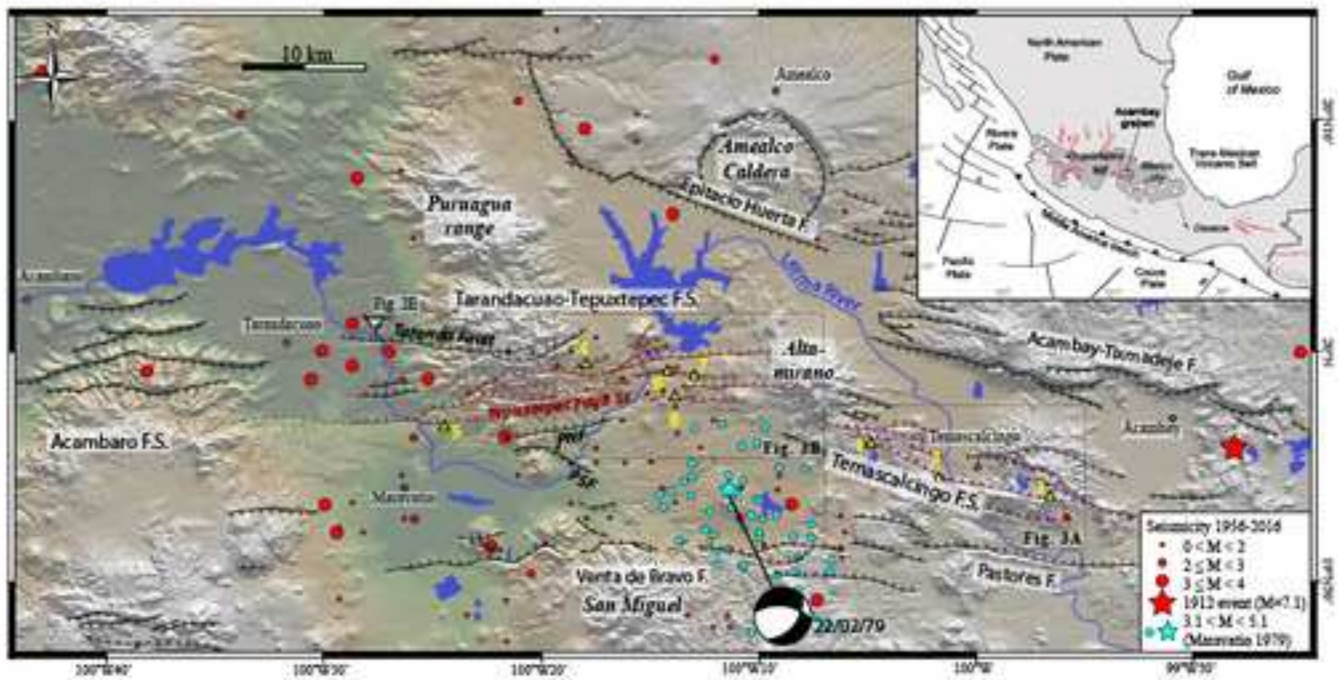

Figure 2a (Color)
Click here to download high resolution image

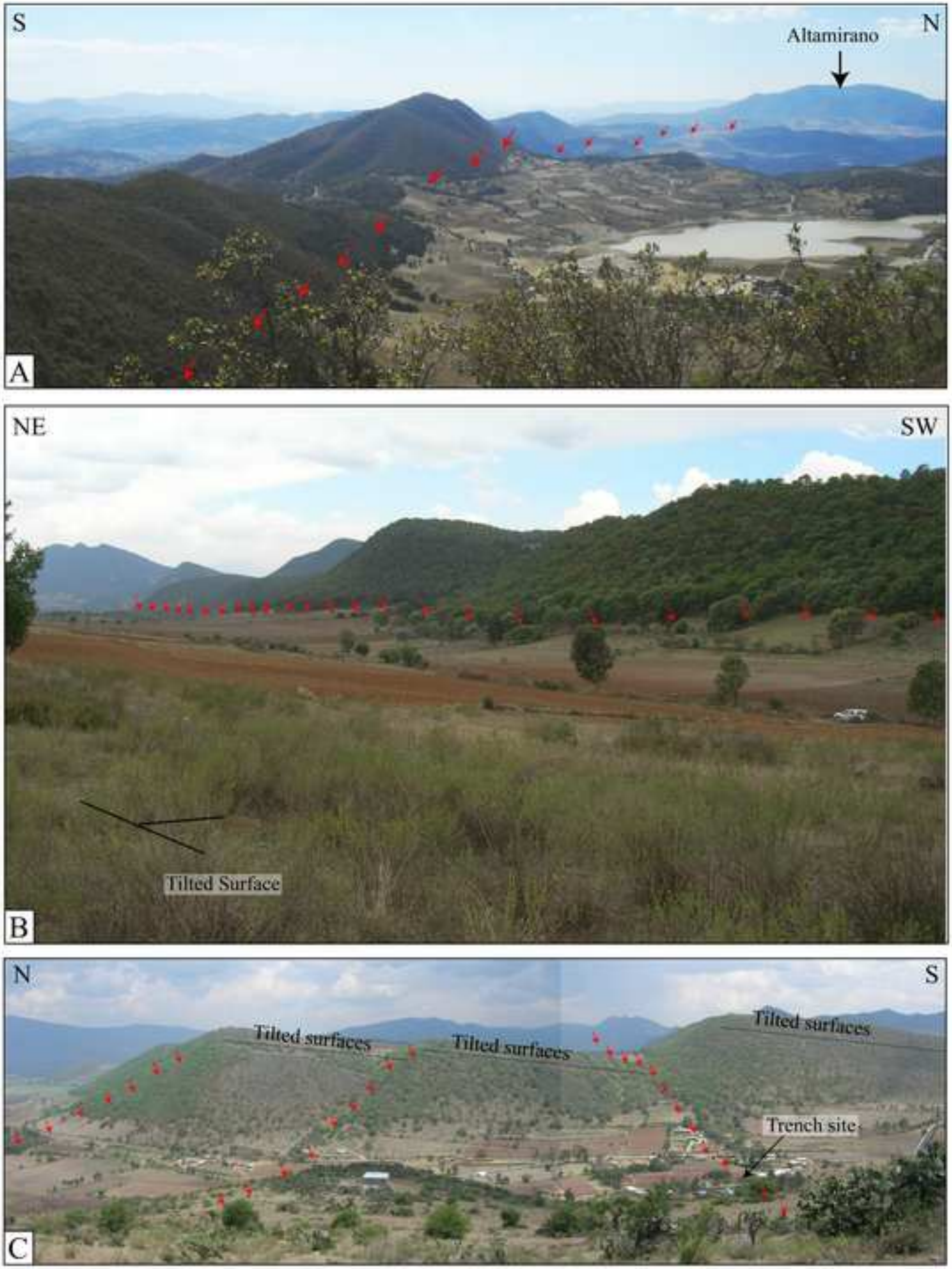

Figure 2b (Color)

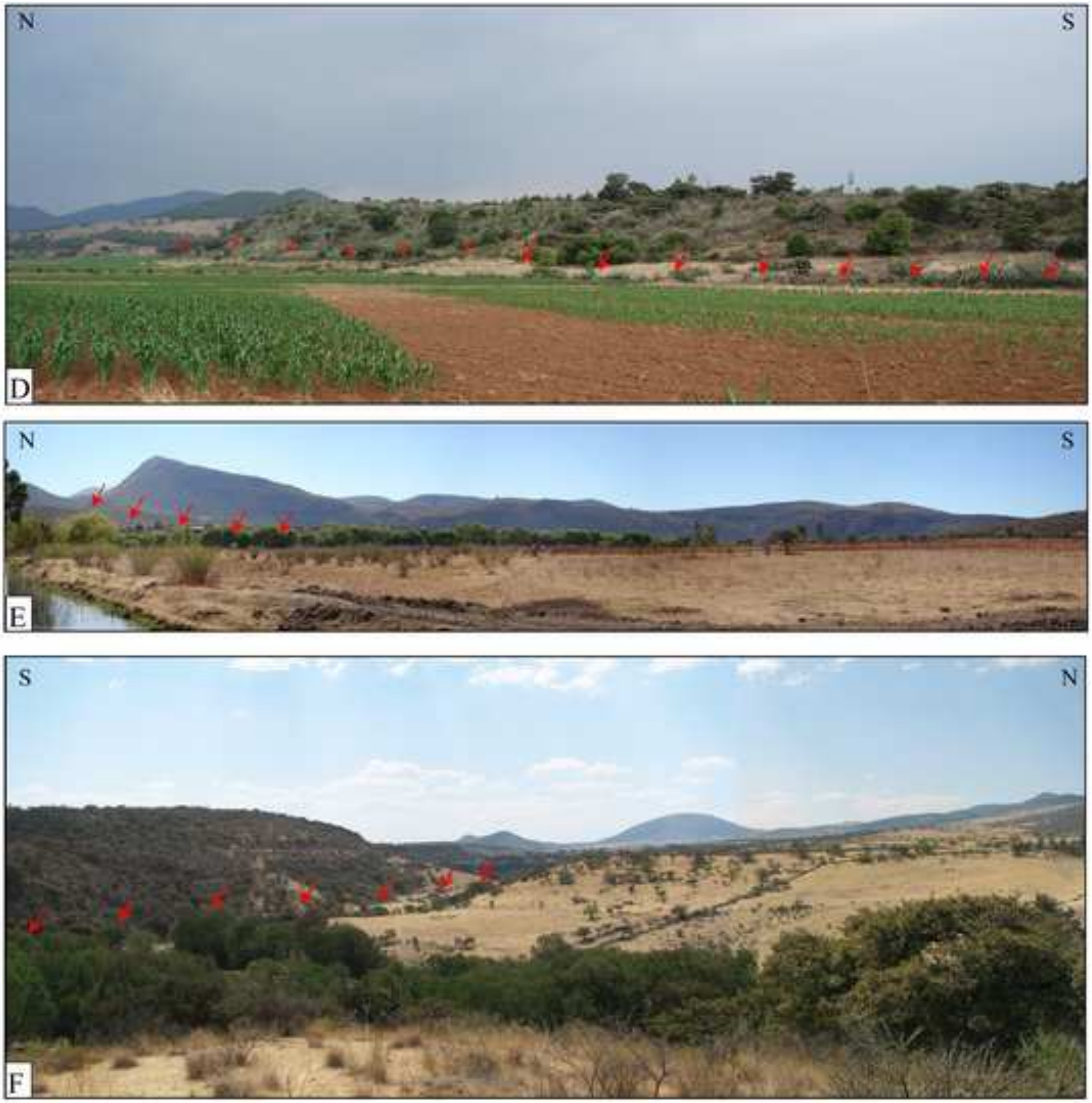

Figure 3 (Color)
Click here to download high resolution image

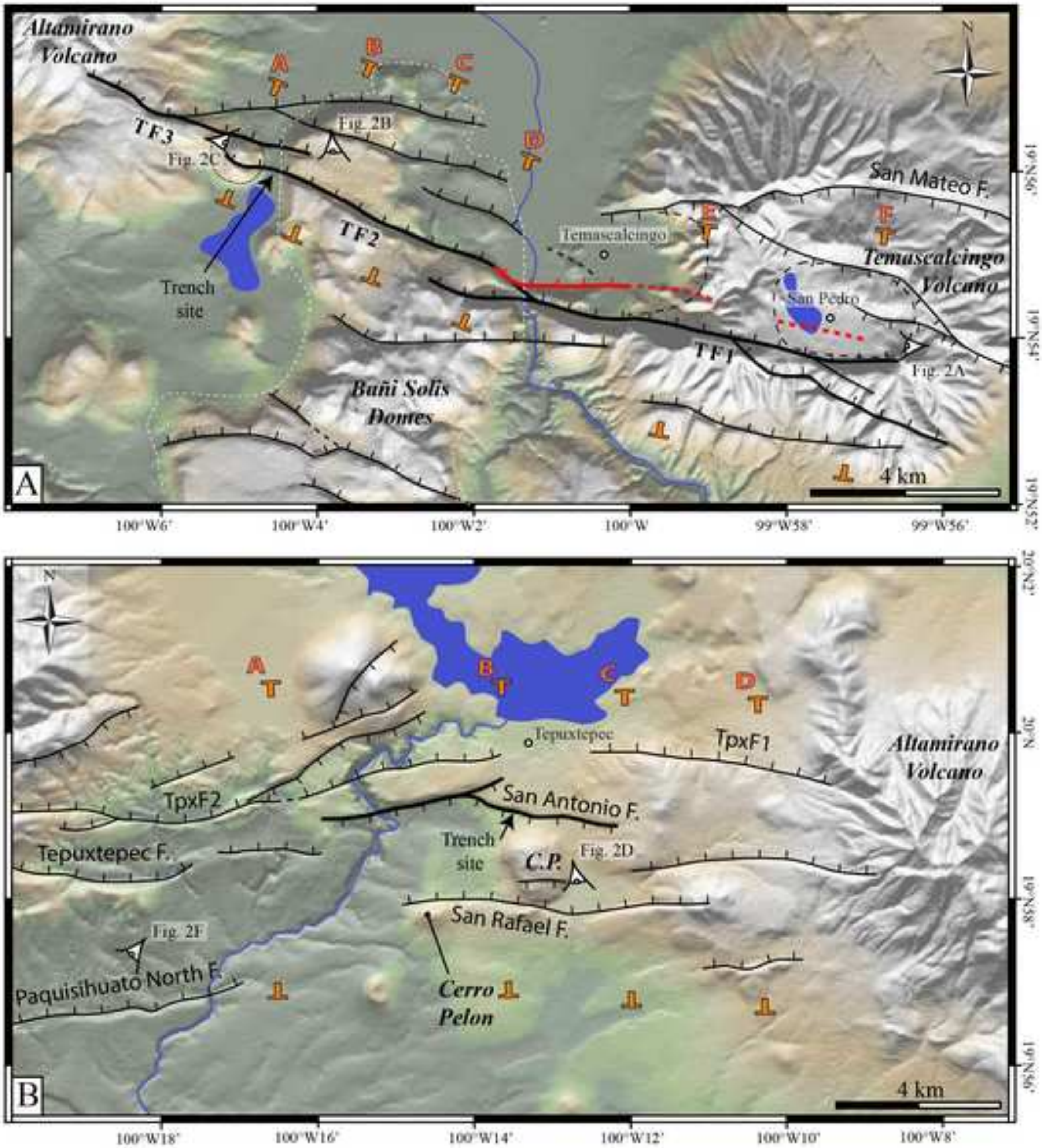

Figure 4 (Color)

Click here to download high resolution image

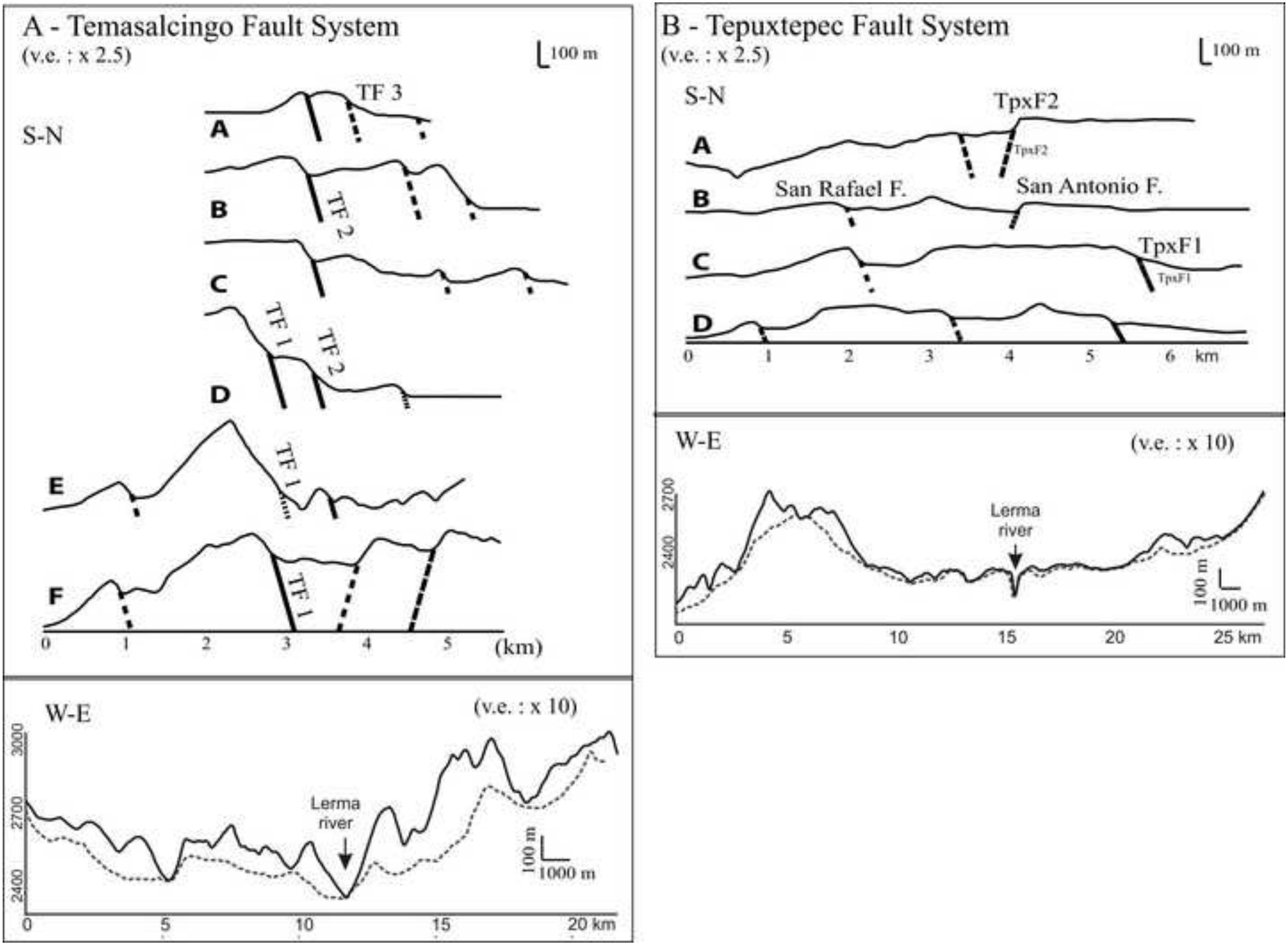

Figure 5a (Color)
Click here to download high resolution image

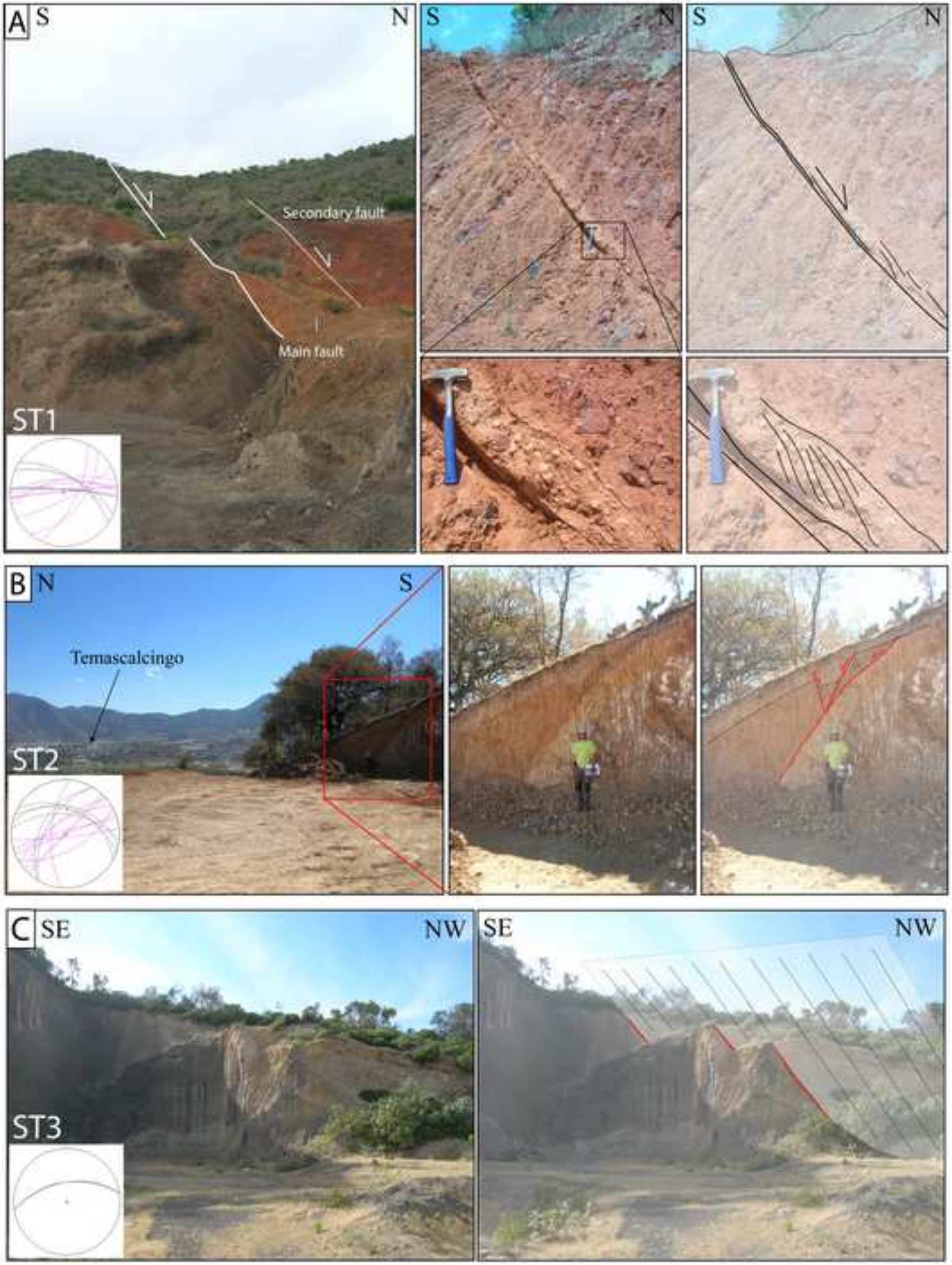

Figure 5b (Color)
Click here to download high resolution image

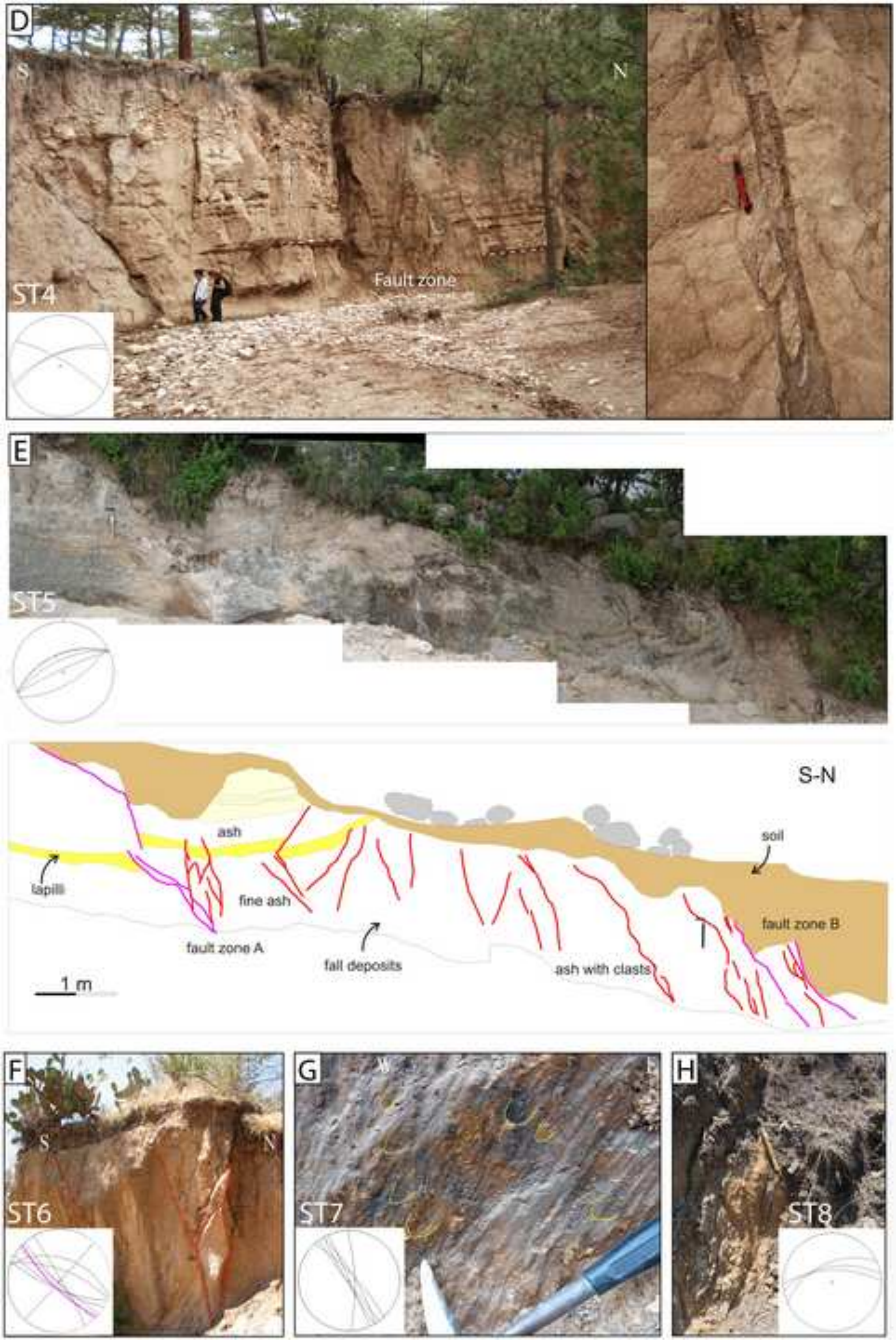

Figure 6 (Color)

Figure 7 (Color)
Click here to download high resolution image

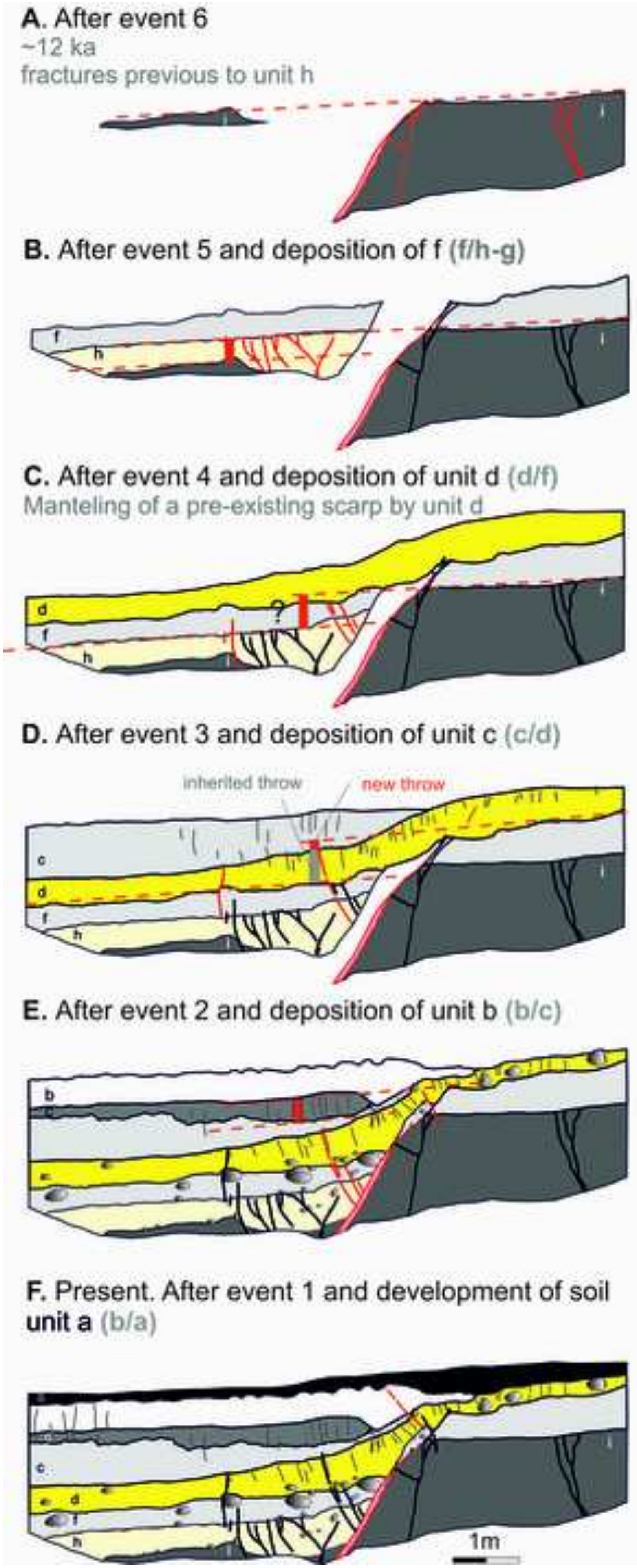

Figure 8 (Color)

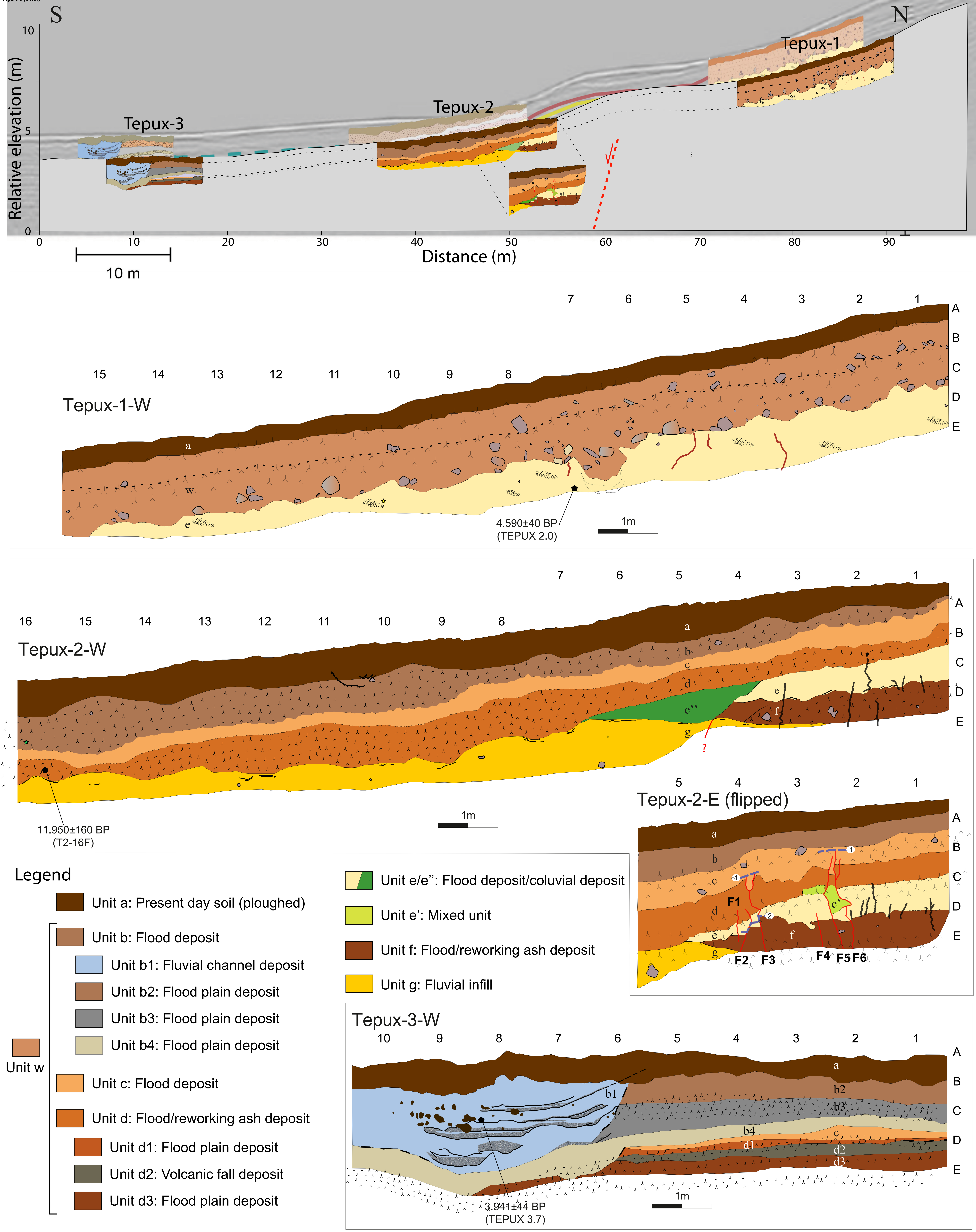

Figure 9 (Color)

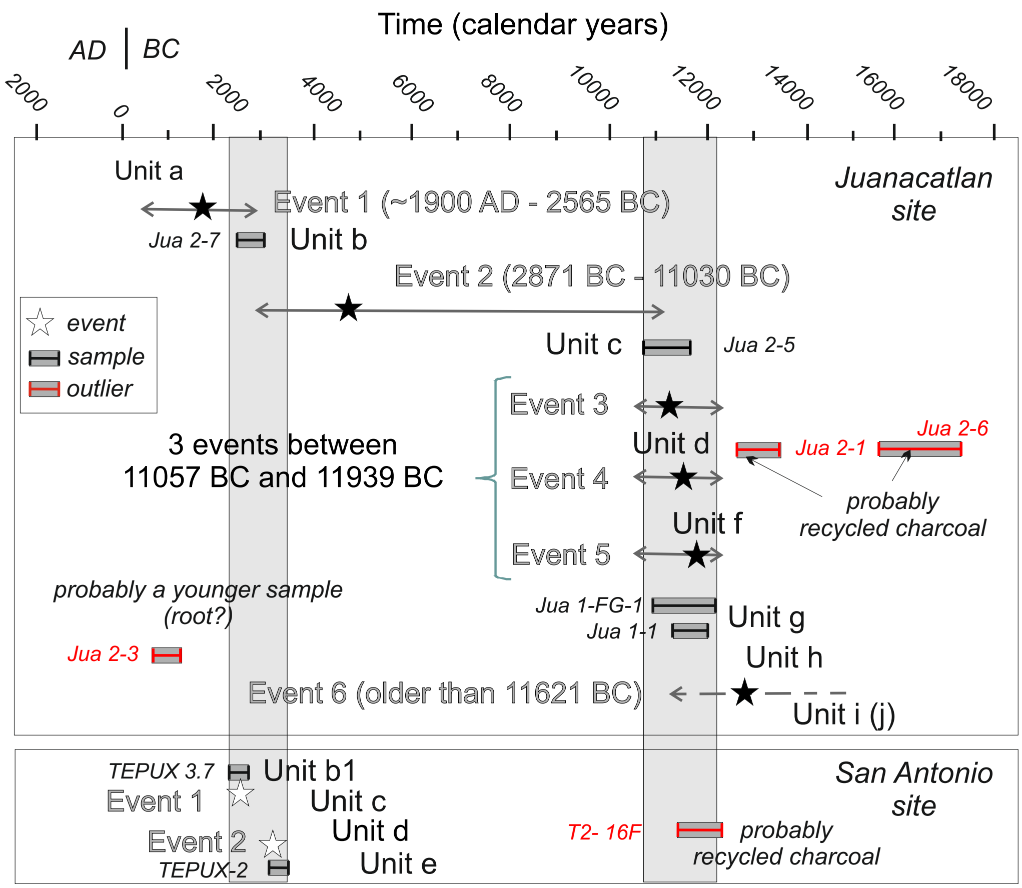

Supplementary material A.1

Click here to download Supplementary material for online publication only: Appendix A1.jpg

Supplementary material A.2

Click here to download Supplementary material for online publication only: Appendix A2.jpg

Supplementary material A.3

Click here to download Supplementary material for online publication only: Appendix A3.jpg

Supplementary material A.5

Click here to download Supplementary material for online publication only: appendix A5.JPG

Supplementary material A.6

Click here to download Supplementary material for online publication only: Appendix A.6.xlsx

Supplementary material A.7
Click here to download Supplementary material for online publication only: Appendix A_7.pdf

Supplementary material A.8

Click here to download Supplementary material for online publication only: Appendix A.8_Juana.oxcal